Ancient Mesoamerica, **31** (2020), 189–209

doi:10.1017/S0956536119000257

DIGITAL IMAGING AND ARCHAEOMETRIC ANALYSIS OF THE CASCAJAL BLOCK: ESTABLISHING CONTEXT AND AUTHENTICITY FOR THE EARLIEST KNOWN OLMEC TEXT

Joshua D. Englehardt,[a] Mirta A. Insaurralde Caballero,[b] Emiliano R. Melgar Tísoc,[c] Luis R. Velázquez Maldonado,[b] Viridiana Guzmán Torres,[c] Henri Noel Bernard,[d] and Michael D. Carrasco[e]

[a]Centro de Estudios Arqueológicos, El Colegio de Michoacán, A.C., Cerro de Nahuatzen 85, C.P. 59379, La Piedad, Michoacán, Mexico
[b]Laboratorio de Análisis y Diagnóstico del Patrimonio, El Colegio de Michoacán, A.C., Cerro de Nahuatzen 85, C.P. 59379, La Piedad, Michoacán, Mexico
[c]Instituto Nacional de Antropología e Historia, Museo del Templo Mayor, Seminario 8, Centro Histórico, Cuauhtémoc, C.P. 06060 Mexico City, Mexico
[d]École doctorale d'Archéologie, Université Paris 1 Panthéon-Sorbonne, Institut d'Art et d'Archéologie, 3 rue Michelet, 75006 Paris, France
[e]Department of Art History, Florida State University, 1019 William Johnston Building, 143 Honors Way, Tallahassee, Florida 32306

Abstract

Although the Cascajal Block (CB), an incised greenstone slab from southeastern Veracruz, Mexico, arguably contains the earliest written text in the New World, debate remains regarding the object's authenticity, dating, and cultural affiliation. To address these issues, this article details recent analyses of the CB via polynomial texture mapping (PTM), X-ray fluorescence (XRF), and scanning electron microscopy (SEM). PTM revealed new details that have resulted in a new epigraphic drawing of the block's incised text and allowed for improved identification of several constituent signs. Spectrometric analysis confirmed that the chemical composition of the CB matrix is consistent with serpentine and identified a uniform patina on its surface, which provided additional contextual data. SEM micrographs of polymer replica molds taken from the incised text evidence manufacturing traces that correspond to lapidary techniques observed on other Formative-period Olmec objects of secure provenience. Results assist in clarifying the archaeological contexts of the object and confirm that in terms of symbols, material, and manufacture the CB conforms to other Formative-period Olmec objects, supporting the object's authenticity, dating, and cultural affiliation.

INTRODUCTION

The 1999 discovery of the Cascajal Block (CB) in southeastern Veracruz, Mexico (Figure 1; Rodríguez Martínez et al. 2006: Figures 1 and 3), provided what is arguably the earliest example of writing in the New World. Although not encountered via systematic excavation, prior studies suggest that the CB is a product of the Olmec culture, and dates to the transition between the Early and Middle Formative periods (~1000 to 800 B.C.; Carrasco and Englehardt 2015; Rodríguez Martínez et al. 2006). These cultural and temporal affiliations are based on three primary data points: (1) the location of the find within the Gulf Coast Olmec heartland, less than 20 kilometers from the major Early Formative-period center of San Lorenzo; (2) the resemblance of the object to the rectangular serpentine slabs recovered from the massive offerings at La Venta Complex A (Drucker 1952; Drucker et al. 1959); and (3) the presence of San Lorenzo-phase ceramic fragments reported to have been contextually associated with the CB (Rodríguez Martínez and Ortiz Ceballos 1999; Rodríguez Martínez et al. 2006:1611).

E-mail correspondence to: jenglehardt@colmich.edu.mx

The polished top surface of the block contains a lightly inscribed text of 62 signs (Rodríguez Martínez et al. 2006:Figures 2 and 4) in a configuration suggestive of writing (Carrasco and Englehardt 2015). Although this script remains undeciphered, previous analyses of the text (Anderson 2012; Carrasco and Englehardt 2015; Freidel and Reilly 2010; Justeson 2012; Macri 2006; Magni 2008, 2014; Mora-Marín 2009, 2010; Rodríguez Martínez et al. 2006; Rodríguez Martínez and Ortiz Ceballos 2007; Skidmore 2006) find the signs consistent with Olmec iconography and several signs from later, seemingly related script traditions. These studies support the theory that writing in Mesoamerica developed from an ancestral Middle Formative-period sign system (Houston 2004; Justeson 2012), likely preserved in part on the CB.

Doubts linger, however, regarding the object's authenticity, dating, and cultural affiliation (Bruhns et al. 2007; Cyphers 2007). These critiques revolve around the object's lack of secure archaeological context and the unique structural properties of the text, which is distinct from the dominant convention of vertical columns characteristic of later Mesoamerican scripts, as well as the singularity of some of its signs (subsequent research, however, showed that the CB signs are consistent with motifs found on

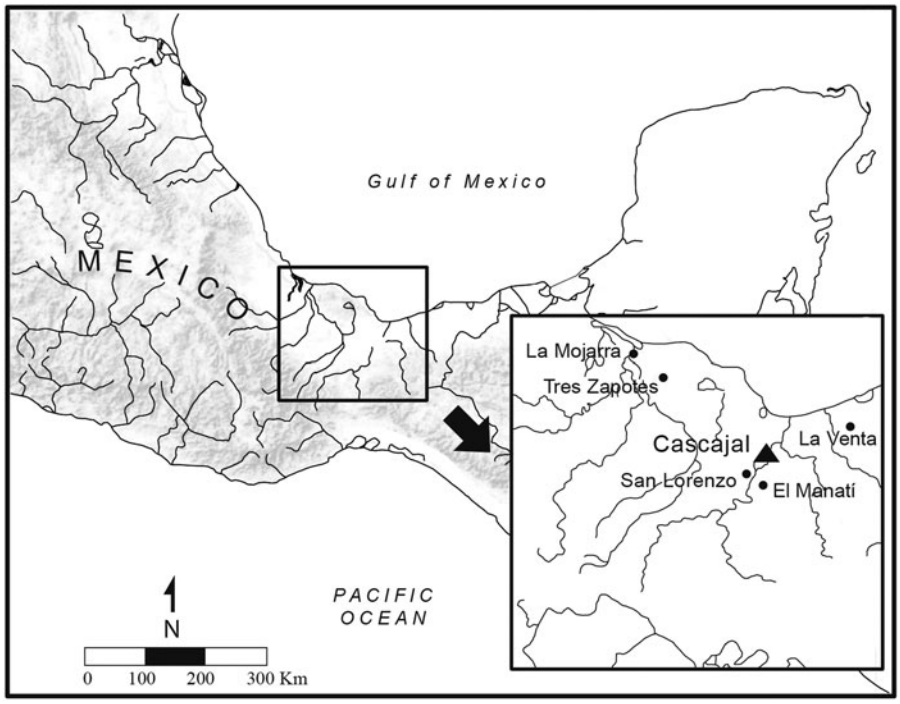

Figure 1. Map detailing location of Cascajal in relation to other Formative-period Olmec sites. Map by Martha A. Soto López, after Rodríguez Martínez et al. (2006:1610, Figure 1).

contemporaneous iconographic materials [Wendt et al. 2014]). Almost all previously published work on the CB has focused on its incised text. Surprisingly, however, no further research on the object itself has been undertaken since the publication of its discovery.

The research from which this article derives was thus designed to produce further data regarding the CB, a singular object of undisputed significance, but one that remains woefully understudied. To achieve this objective, several non-destructive methods and techniques were employed: (1) PTM computational photography; (2) XRF spectrometric analysis; (3) the analysis of manufacturing traces via optical and SEM of polymer replica molds that reproduced the surface microstructure of the CB's incised text; and (4) comparative analysis of tool marks revealed through SEM analysis with micrographs of experimentally produced reference specimens and other objects of known archaeological context or recognized authenticity that had been previously analyzed following the same methodology.

This article reports and discusses these recent analyses of the CB. Results show that the CB is consistent with other Formative-period Olmec artifacts of known context in terms of material and manufacture. Further, results provide supplementary evidence that clarify the archaeological contexts and dating of the object, strengthening arguments in support of its authenticity and cultural affiliation. These findings allow us to place the CB firmly within the larger context of Olmec cultural traditions and bolster previous interpretations of the object as the first known example of writing in the New World.

PTM

PTM, also known as reflectance transformation imaging (RTI), is a computational image capture and processing technique developed by Hewlett-Packard Laboratories that yields high-quality photorealistic renderings of a textured surface (Earl et al. 2010; Malzbender et al. 2001). The technique records the shape, color, and reflectance functions of an object's surface and enables the interactive relighting of the subject from any direction under variable conditions (e.g., different angles, intensity, or wavelength), as well as the mathematical enhancement of surface attributes, since the appearance of a surface varies with lighting conditions (CHI 2018; HP Labs 2019a). PTMs reveal subtle surface details difficult to observe via standard photography or direct empirical examination. The technique has been deployed in a variety of contexts to aid archaeological investigations of incised surfaces (e.g., Diaz-Guardamino and Wheatley 2013; Purdy et al. 2011).

Following the best practices for image capture outlined by Cultural Heritage Imaging (2011), a series of 48 images of the CB was captured with a Canon Electro-Optical System (EOS) 70D digital single-lens reflex camera fitted with a Canon EF-S 60 mm f/2.8 Macro USM prime lens, fixed to a Manfrotto MH804-3WUS 3 Way head, mounted on a Manfrotto MT290XTC3US 290 Xtra 3-Sec Carbon Tripod. Flash lighting was provided by a Yongnuo Speedlite YN560-III. To avoid movement, images were captured by triggering the camera and flash remotely using Canon's EOS utility and Digital Photo Professional 4.6.30 software. Photos were captured in RAW format at 25.3 MB per file, with camera settings of f/9, an exposure time of one second, ISO-100, 60-mm focal length, 0 exposure bias, and manual focus. The flash was set at a speed of 1/128 with a 60-mm focal length. Two reflective spheres were included in each shot, as the reflection of the light source on the spheres enables the processing software to calculate the light direction for that image and model view-specific, per-pixel reflectance functions. An X-Rite ColorChecker was also included in each shot to ensure

https://doi.org/10.1017/S0956536119000257 Published online by Cambridge University Press

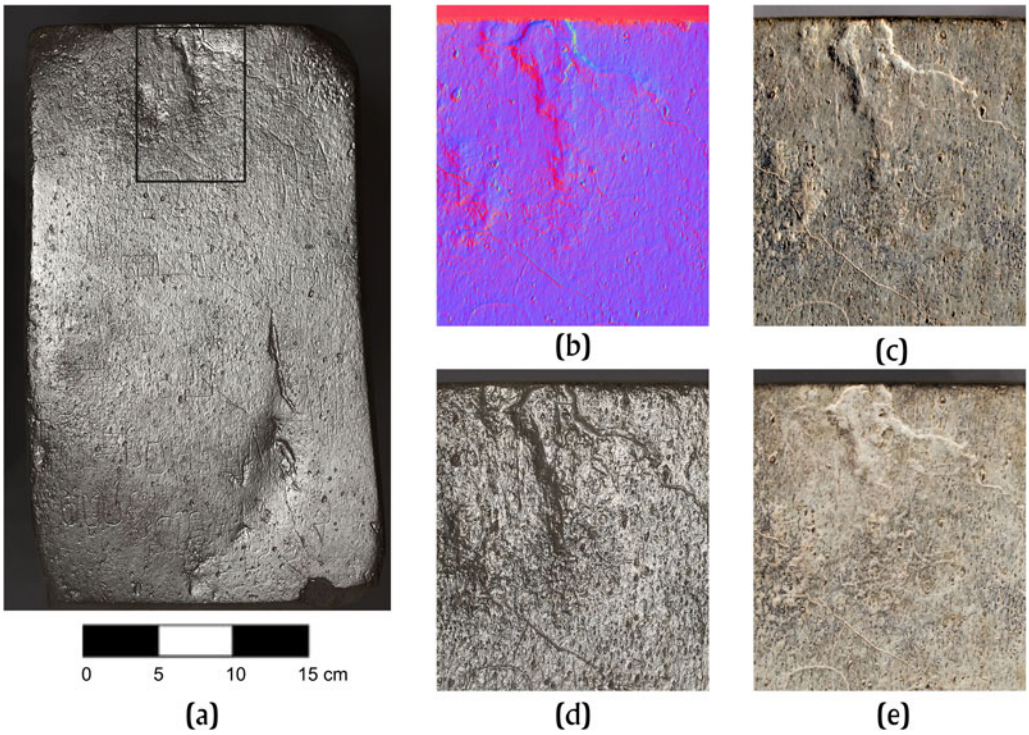

Figure 2. (a) Polynomial texture mapping of the Cascajal Block, showing improved resolution surface details via distinct visualization modes of outlined area. (b) Normals. (c) Dynamic multi-light. (d) Specular enhancement. (e) Image unsharp masking.

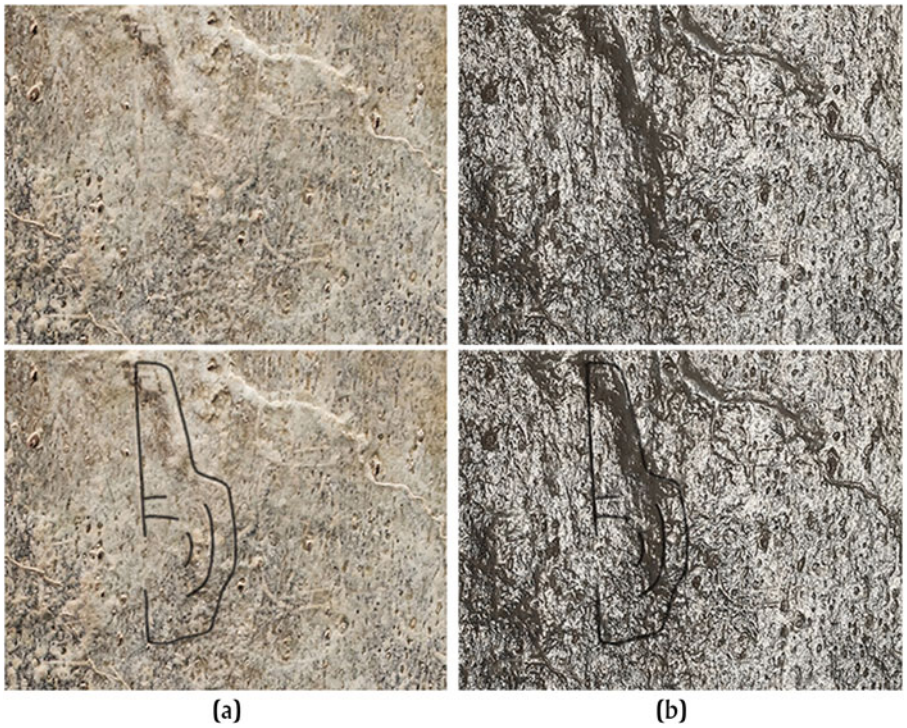

Figure 3. Identification of sign 5 in top row of the Cascajal Block text as CS16 via polynomial texture mapping visualization modes. (a) Image unsharp masking (gain = 35). (b) Specular enhancement (diffuse color = 40, specularity = 80, highlight size = 75). Additional sign detail superimposed (bottom row; cf. Rodríguez Martínez et al. 2006:1612, Figure 4). All references to CS numbers follow the numbering scheme of the sign inventory proposed by Rodríguez Martínez et al. (2006:1613, Figure 5).

https://doi.org/10.1017/S0956536119000257 Published online by Cambridge University Press

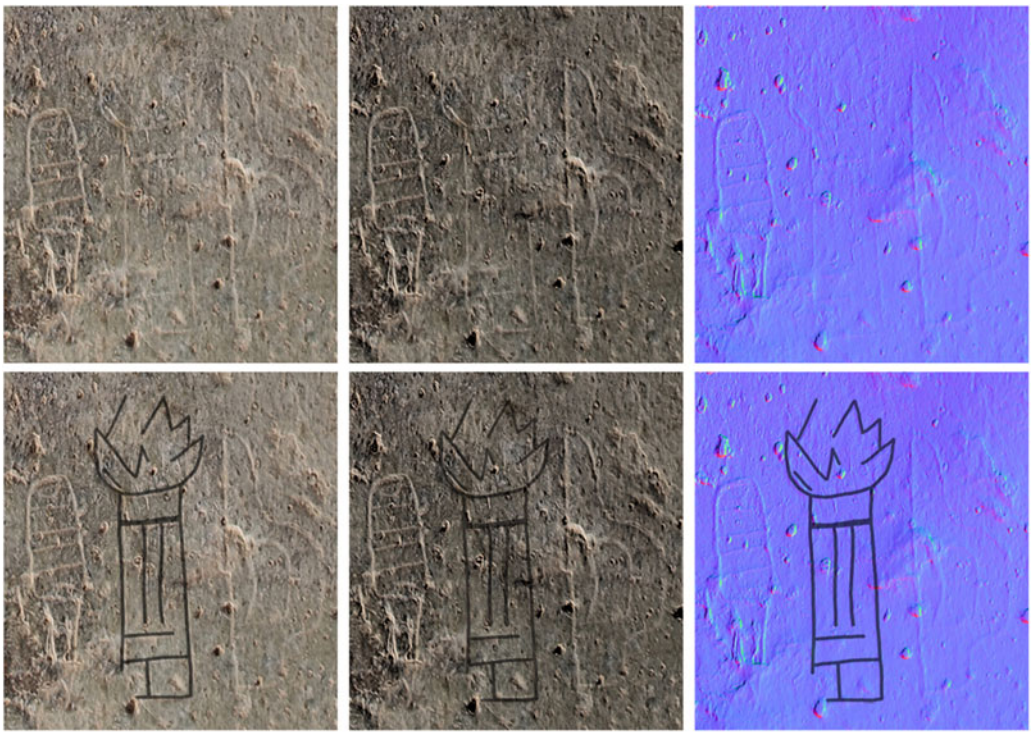

Figure 4. Identification of sign 57 in bottom row of the Cascajal Block text as CS12 via polynomial texture mapping visualization modes. (a) Dynamic multi-light (tile size = 32 px, offset = 15°). (b) Diffuse gain (= 25). (c) Normals. Additional sign detail superimposed (bottom row). Note the vegetal motifs emerging from the bundle, which are distinct from the circular element depicted atop this sign in previous drawings (cf. Rodríguez Martínez et al. 2006:1612, Figure 4).

correct exposure, color, and white balance. RAW images were first adjusted as necessary with the Adobe Camera Raw tool in Adobe Lightroom, and then converted into digital negatives (DNG) for archiving via the open-source Adobe DNG converter V.11.1 (Adobe Systems 2019). Finally, DNGs were batch converted to JPEGs in Lightroom for processing in RTI and PTM builder software.

These images were then processed on a Dell XPS 8700 with an Intel Core i7 3.60 GHz processor, running a 64-bit Windows 7 Pro OS, following processing routines provided by Cultural Heritage Imaging (CHI 2013). We used CHI's (2017) RTI Builder software, with the open-source HP PTM Fitter plugin (HP Labs 2019b). This program is a software interface to a set of tools that process captured image sets to produce RTI or PTM files. The variable lighting conditions are read into the program, light positions are automatically identified and manually adjusted as necessary, and the processing sequence algorithm generates the reflectance image. PTMs offer a variety of interactive viewing options, including specular enhancement, dynamic multi-light, and normals visualization. RTI Builder software is available under the Gnu General Public License V.3.0. RTI and PTM files may be viewed in a variety of open-source programs, such as CHI's RTI Viewer.

The PTM we created reveals surface details not evident in previously published images or drawings of the CB (Figure 2). Although such details may not be immediately evident in the full PTM image of the CB's inscribed surface (Figure 2a), they are highlighted through the distinct rendering modes in the RTI Viewer program (Figures 2b–2e, 3, and 4). These details assist considerably in the accurate identification of the text's constituent signs by bringing out aspects difficult to detect even in ultra-high-resolution macro photography. Further, PTM imagery also assists in evaluating qualitative differences among the incisions, and distinguishing intentional cuts from other surface marks, such as naturally occurring pits or cracks along the object's surface (see Mora-Marín 2020: Figure 3). Such determinations, in turn, may aid in the detection of possible earlier inscriptional strata.

Rodríguez Martínez and colleagues (2006:1612) hypothesize that the CB text was "an erasable document that could be removed and revised" (see also Ortiz Ceballos et al. 2007:18). No examples of such palimpsests have been presented to date, however. Mora-Marín (2020:Figure 5), using our PTM data, has identified an area in the upper right corner of the CB that may show "a leftover portion of an earlier layer of material," which would support the previous hypothesis. We have also detected areas that may evidence an earlier stratum of inscription (Figure 5) and complement Mora-Marín's suggestion. In the second row of the upper central portion of the block, we noticed several marks between CS18 and CS10. These lines appear to be of similar thickness to the current incisions, but are noticeably fainter. Another mark crosscuts the parallel lines to the lower left at a 45° angle (shown slightly fainter in lower right of Figure 5). This mark, however, appears distinct from both those of the possible palimpsest and the current inscription, and may simply be a scratch on the object's surface. We had previously noted several similar marks, particularly concentrated on the upper left portion of the CB around CS6 and CS9 in the second row of inscriptions

https://doi.org/10.1017/S0956536119000257 Published online by Cambridge University Press

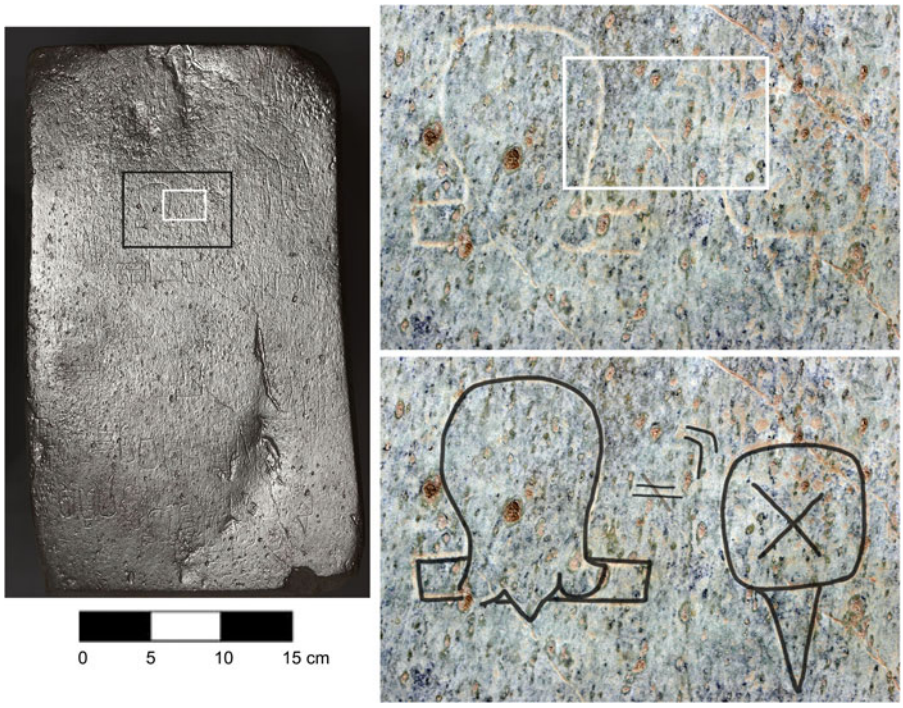

Figure 5. Possible evidence of an earlier inscriptional stratum on the Cascajal Block. Note the relatively fainter marks between CS18 and CS10.

(Englehardt et al. 2017:353, Figure 1). In the end, however, these examples are far from conclusive. The possible earlier stratum noted by Mora-Marín (2020:Figure 5), for example, presents marks that are noticeably distinct from the other incisions, insofar as the incised lines in this area appear significantly deeper and thinner than the incisions in the sign immediately to their left.

Figure 6. Possible abrasion marks on the surface of the Cascajal Block, as seen in polynomial texture mapping specular enhancement mode (diffuse color = 40, specularity = 70, highlight size = 25). Note the fine lines and diffuse bands running diagonally from the upper left to lower right within the three highlight boxes.

The high-resolution examination of the inscribed surface via PTM does, however, reveal marks that appear to have been the result of surface reduction, possibly abrasion (Figure 6; cf. Mora-Marín 2020:Figure 3). Subsequent analysis of similar marks on other CB surface areas (see Analysis of Manufacturing Traces) indicates that these marks are most likely the result of abrasion with sandstone. These diffuse bands and fine lines appear in some cases to have been intentionally overwritten by inscribed signs. For example, parts of the incisions for CS28 and CS24 (middle highlight box in Figure 6) crosscut these bands and lines, which would strongly suggest that they were inscribed after surface abrasion. Whether such reduction was to erase an earlier inscription or simply to prepare the object's surface for the current text is unknown. On the other hand, some marks are clearly superimposed over the current inscription, although these may simply be scratches or cracks that postdate the inscription. More specific analyses of these marks and their evaluation against known standards—possibly via the traceological techniques discussed in Analysis of Manufacturing Traces—are necessary to fully assess these examples.

PTM imagery also exposes what appear to be uneven wear patterns. These are particularly evident along the right side of the block, where inscriptions appear fainter and less well-defined—visible even in previously published photos (e.g., Rodríguez Martínez et al. 2006:1611, Figure 2). These patterns may suggest abrading and polishing to erase marks at particular locations on the object surface, which would also support the hypothesis of the text as erasable (since repeated abrading and polishing to erase marks at particular surface locations would have produced variable

https://doi.org/10.1017/S0956536119000257 Published online by Cambridge University Press

weathering patterns). Alternately, they may indicate a particular kind of wear, which could provide insight into the object's use after it was inscribed. Ultimately, however, inspection of the CB surface via PTM does not corroborate these or other previous suggestions. While the hypothesis of the CB text as an erasable, revisable document remains a possibility, PTM imagery does not reveal definitive indications of palimpsests, other marks belonging to earlier inscriptional strata, or evidence for the existence of multiple hands in the creation of the text—although some inscriptions appear to be more deeply incised. Further mineralogical and traceological analysis of the surface may provide additional data that allow for a more definitive resolution of these questions.

On the basis of the PTM, we created a new epigraphic drawing of the CB text (Figure 7; cf. Mora-Marín 2020:Figures 3 and 4). The PTM imagery that informs this drawing allows for the addition of details not previously recorded (cf. Rodríguez Martínez et al. 2006:1612, Figure 4), which enhances our understanding of specific signs. For example, the identification of Sign 5 (CS16, fifth from left in the top row of Figure 7; see Figure 3) as the common Olmec knuckleduster motif, or Sign 57 (CS12, eighth from left in the bottom row; see Figure 4) as a vegetal bundle or torch, another visual element common in Middle Formative-period iconography. We also noticed an oval motif inset in Sign 14 (CS3, extreme right in the second row). Mora-Marín (2020:Figure 6) has also revised the identification of Sign 3 (third from left in the top row) as CS15, and not CS27, as previously documented. Although we had not initially noticed this detail, we concur with Mora-Marín's identification, and have accordingly revised our own drawing.

Although these new details may seem relatively minor, precise identification of the signs that constitute the CB text is crucial to constructing a deeper understanding of early texts for which we have but a few examples. For instance, such specificity directly impact proposals regarding reading order and sign groupings, or the presence of structural properties that potentially suggest linguistic organization, such as those suggested by Carrasco and Englehardt (2015), Justeson (2012), Macri (2006), Mora-Marín (2009), Rodríguez Martínez et al. (2006), and others. In addition, accurate identification of inscribed features assists in proposing specific decipherments (e.g., Carrasco and Englehardt 2015:649) and generating hypotheses for future research, as suggested above (also see Mora-Marín 2020). Finally, more precise identification and understanding of iconographic details can also advance interpretations of archaeological objects, as in Wendt et al.'s (2014:312) discussion of the scallop incision on CS1 (Signs 2, 24, 38, and 52 in the CB text). Thus, in the case of the CB, the additional detail, identification, and confirmation of Middle Formative-period motifs in the text further argues for the object's dating and cultural affiliation, complementing the results of the archaeometric analyses discussed in the following sections.

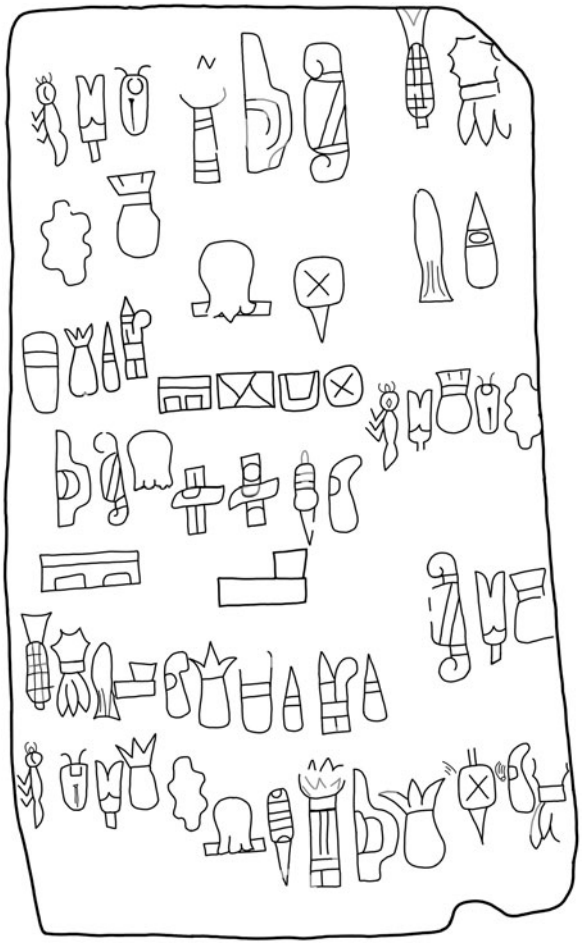

Figure 7. New epigraphic drawing of the Cascajal Block text. Drawing by Michael D. Carrasco.

XRF SPECTROMETRY

Previous investigations (Robles Camacho et al. 2008; Rodríguez Martínez et al. 2006), as well as superficial visual examination, suggest that the mineral matrix of the CB is serpentine. To further corroborate this identification, we focused on characterizing the CB via a qualitative and quantitative chemical study of its multielemental composition using portable dispersive energy X-ray fluorescence spectrometry (pXRF). Eight areas (Online Appendix 1) on the inscribed surface and sides of the CB were irradiated and analyzed. These results were then comparatively analyzed against the XRF characterization of five mineral samples: three of serpentine (one from Río Verde, Oaxaca and two from Tehuitzingo, Puebla), one of jadeite from the Motagua Valley, Guatemala, and one of green quartz from Mezcala, Guerrero. To ensure that these reference specimens were correctly characterized, thin sections of the samples were analyzed with an Olympus BX41 Petrographic Microscope in the Laboratory for Research and Characterization of Materials and Minerals (LICAMM) at the University of Guanajuato (see Puy y Alquiza 2017). Further, X-ray diffraction (XRD) was also employed to characterize the samples, using LICAMM's Rigaku Ultima IV diffractometer, which revealed the structure and crystalline phases of the material analyzed. These mineralogical identifications of the samples served as points of reference to reinforce and ratify the results obtained via pXRF.

The pXRF analysis of the CB and mineral samples was performed with a Thermo Fisher Scientific NITON XL3t GOLDD+ portable spectrometer. The following analytical conditions were implemented: irradiation time = 60 s, I = 40 μA, U = 50 kV, spot size = 8 mm, and number of measurements = 8 for the CB and 3 for the five samples of serpentine, quartz, and jadeite, respectively.

Quantitative data was obtained through two episodes of irradiation at each sampled area, in two analytic modes: "Test All Geo" and "Soils" (Velázquez Maldonado 2017:70–96). Due to the characteristics of this particular spectrometer (Thermo Fisher Scientific 2011),

https://doi.org/10.1017/S0956536119000257 Published online by Cambridge University Press

the chemical determination was based on four irradiation stages: Main, High, Low, and Light. In the qualitative analyses, the pXRF spectra of the Main, High, and Low stages of the "Soils" mode were analyzed, since they presented a higher intensity than their "Test All Geo" mode counterparts. For the Light stage, the spectrum linked to the "Test All Geo" mode was used.

The pXRF spectra of the Main stage of irradiation (Figure 8) reveal that the CB matrix presents significant similarities to chemical signatures of the serpentine samples, specifically in terms of the peak intensities (Kα and Kβ) of the elements Ca (Figure 8a), Cr and Mn (Figure 8b), Fe (Figure 8c), and Sr, Y, and Zr (Figure 8d). These data also reveal significant differences in the chemical composition of the CB matrix with respect to the samples of quartz and jadeite. The pXRF spectra from the High, Low, and Light irradiation stages (Figures 9–11) corroborate these results, revealing chemical differences between the CB and serpentine samples with respect to other greenstone mineral samples. Spectral dissimilarities are evident in discrete peak intensities for elements such as Ca (Figures 8a, 9, 10a, 11c), and Cr, Mn, Fe, and Ni (Figures 8b, 9, 10b, and 11d), in addition to other differences associated with the elements Sr, Y, and Zr (Figures 8d and 9a).

Conversely, the data show significant similarities between the CB matrix and serpentine. These are expressed by the peak intensity values for the elements Ca (Figures 8a, 9, 10a, 11a, and 11c) and Fe (Figures 8c, 9a, b, 10b, 11b, and 11d), as well as in the presence of Cr, Mn, and Ni in both the CB matrix and the serpentine samples (Figures 8b, 9, and 10b). Cr, Mn, and Ni may be considered diagnostic elements for the geological attribution of the CB elemental matrix, since they occur in concentrations representative of the chemical composition of ultramafic rocks (Fandeur et al. 2009; Mercy and O'Hara 1967; Oze et al. 2004). Deposits of serpentine in Mexico, linked to ultramafic-mafic formations, exhibit the same chemical characteristics (Ortiz et al. 2006).

Finally, the CB matrix displays a nearly identical chemical signature to the samples from the Tehuitzingo, Puebla deposit, and a slight difference with the serpentine sample from Río Verde, Oaxaca. The latter presents a notably higher peak intensity for Zr (Figure 9a), not evident in the CB or other serpentine samples.

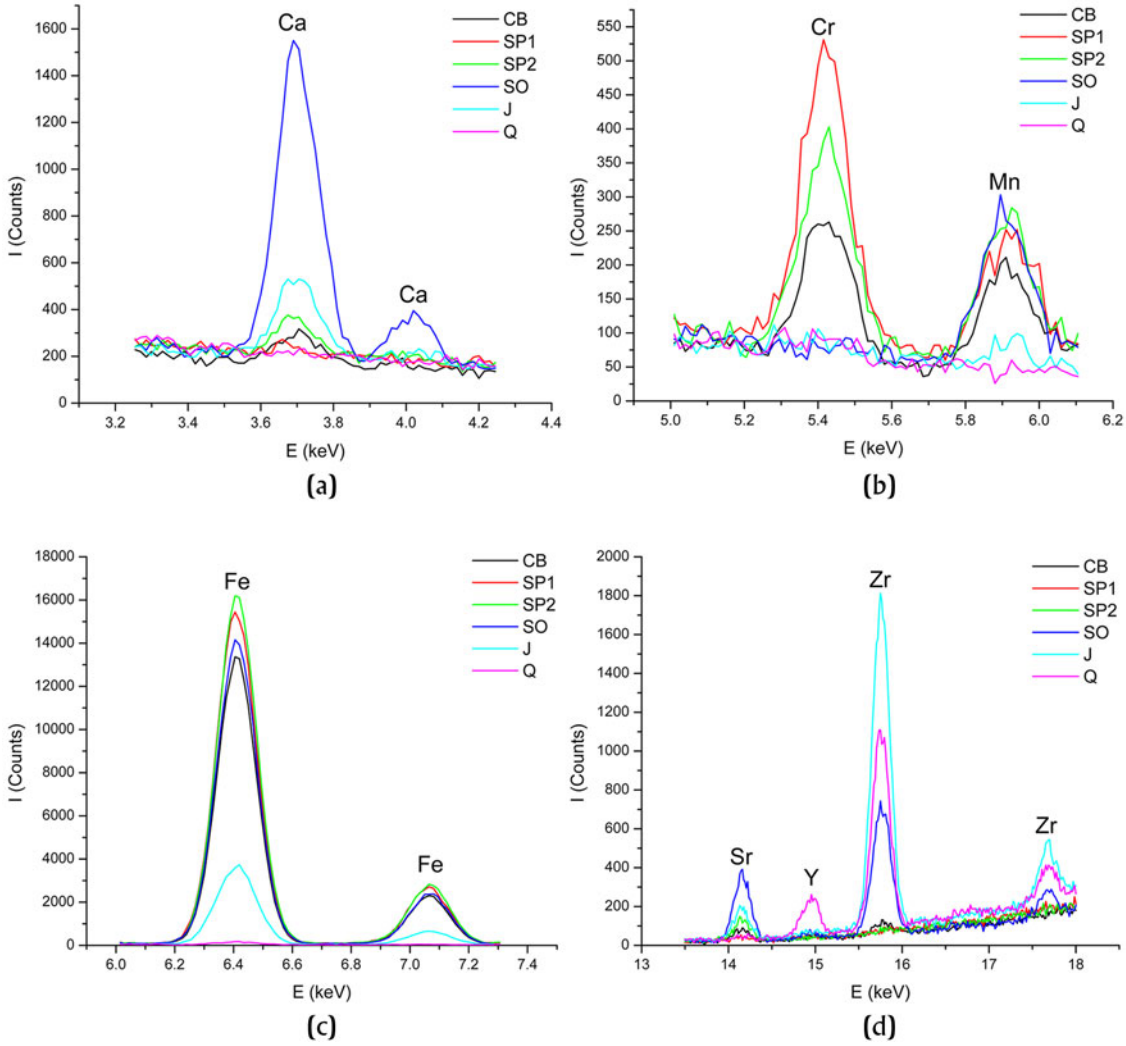

Figure 8. Portable dispersive energy X-ray fluorescence spectrometry spectra corresponding to the Main stage of irradiation. CB, Cascajal Block; SPI and SP2, Puebla serpentine; SO, Oaxaca serpentine; J, jadeite; Q, green quartz.

https://doi.org/10.1017/S0956536119000257 Published online by Cambridge University Press

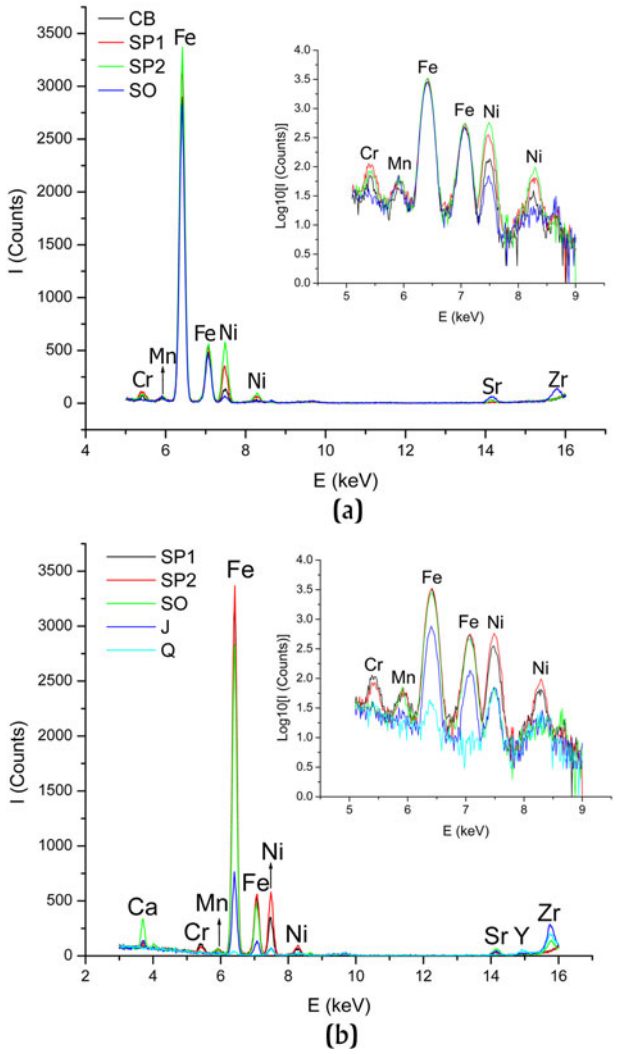

Figure 9. Portable dispersive energy X-ray fluorescence spectrometry spectra corresponding to the High stage of irradiation. CB, Cascajal Block; SPI and SP2, Puebla serpentine; SO, Oaxaca serpentine; J, jadeite; Q, green quartz.

These data suggest that the source of the CB material matrix may be Tehuitzingo. Superficial visual comparison of the surface color and patination patterns of the CB matrix with Tehuitzingo serpentine support this proposal. Tehuitzingo has been identified as a common source of the material in the Formative period, particularly among Olmec cultural groups (Robles Camacho et al. 2008). It would therefore be unsurprising if the material used to fabricate the CB came from Tehuitzingo. Further analysis of mineral and spectrometric samples from that source (and others), however, is needed to confirm this suggestion.

The qualitative data thus reveal the CB matrix is, in terms of chemical composition, nearly identical to serpentine, supporting its previous identification as serpentine. Although a superficial resemblance between the CB and serpentine is visually apparent, pXRF analysis adds additional evidence to support this characterization. Nonetheless, spectrometric data speaks to the identification of chemical elements, not a particular mineral, such as serpentine. In this sense, the pXRF data proves only that the CB matrix is chemically more similar to serpentine than it is to other greenstones commonly used in pre-Hispanic Mesoamerica. While this characterization is significant, to identify a mineral matrix with certainty, XRD is more appropriate. Anomalous readings discovered in the analysis of the pXRF spectra, however, assist in substantiating the characterization of the CB matrix as serpentine and provide additional data regarding its source, as well as clues concerning the object's context and dating.

A Diffraction Signal in the pXRF Data

In the pXRF spectra of the Light irradiation stage (Figure 11) for the chemical signatures of the serpentine sampled from the Tehuitzingo, Puebla, deposit, we encountered a signal located at 4.47 keV (Figure 12), which cannot be assigned to any radiation characteristic of XRF or distinct satellite lines. Curiously, the shape of this peak differs significantly from the usual form present in lines characteristic of XRF, while it coincides with the perfect Gaussian form described for diffraction signals (Alfonso et al. 2002). We thus infer that this is, in fact, a diffraction signal. Notably, this signal is not evident in the serpentine from Río Verde, Oaxaca. The peak between 4.3 and 4.75 KeV in Figure 12 corresponds to the XRF identification of Ti in the Oaxaca sample. This fact, in turn, indicates that the signal derives from a crystalline structure and not from chemical composition, since its presence in the spectrum is conditioned by the orientation of the cut made for the separation of the piece that constitutes our sample.

The presence of diffraction signals in fluorescence spectra is not entirely unusual, and has been reported in the scientific literature (e.g., Mendoza Cuevas and Pérez Gravie 2011). These authors report that, theoretically, the relationship between the energy at which the signal appears and the interplanar distance it represents may be calculated according to following equation:

$$\mathrm{E\ d\ sen}\theta = 6.19926\ \mathrm{keV\AA}$$

This equation applies only to cases in which both the angle of incidence of the primary radiation (θ_1) and the angle of output of the radiation detected (θ_2) are equal. In the geometric conditions of analysis associated with the portable spectrometer employed in this study, however, these values are distinct: $\theta_1 = 71°$; $\theta_2 = 61°$ (Steyn 2014:17; Thermo Fisher Scientific 2011). Thus, we developed the following equation to determine interplanar distance:

$$\mathrm{E\ d}(\mathrm{sen}\theta_1 + \mathrm{sen}\theta_2) = 12.39852\ \mathrm{keV\AA}$$

This results in a calculated interplanar distance of 1.52 Å. Various studies (e.g., Bailey 1969; Esteves 2016:132; Fryer and Mottl 1992) report this interplanar distance as an identifying characteristic of serpentine.

This interplanar distance is not, however, one of the fundamental characterization signals of serpentine, which are 7.3 Å, 3.64 Å, and 2.52 Å (Valdivia et al. 2014). These distances are identifiable in XRF spectrums in energy signals at 0.93, 1.87, and 2.7 keV, respectively. In this case, however, such XRD peaks are not observable via XRF, since they occur in a low-energy range. Such low ranges present analytic difficulties for the spectrometer we employed, and the XRD peaks would therefore overlap XRF signals, such as occurs at the distance of 2.57 Å, which encounters interference with the Kα peak of Cl.Nonetheless, the interplanar distance we calculated does provide an additional data point for the identification of the CB mineral matrix and its source.

https://doi.org/10.1017/S0956536119000257 Published online by Cambridge University Press

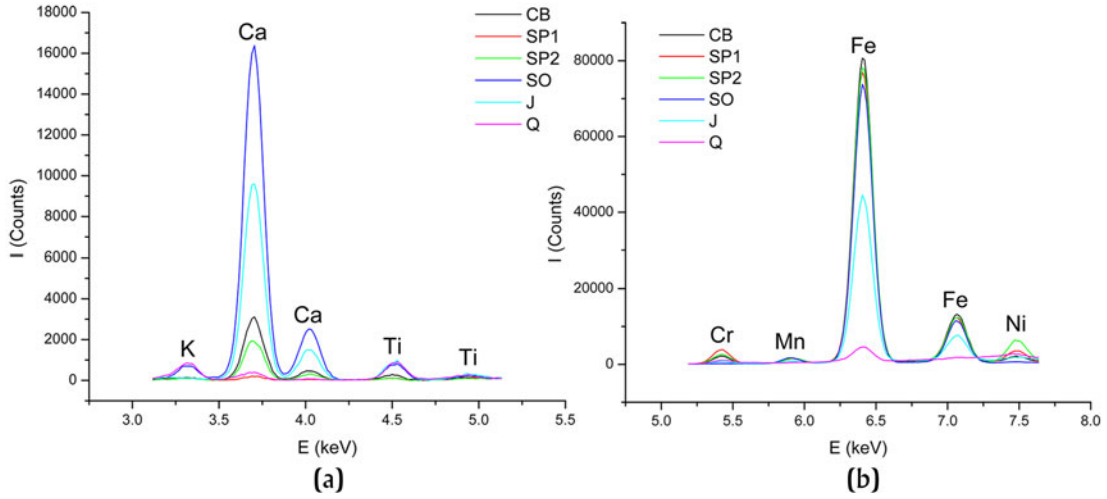

Figure 10. Portable dispersive energy X-ray fluorescence spectrometry spectra corresponding to the Low stage of irradiation. CB, Cascajal Block; SPl and SP2, Puebla serpentine; SO, Oaxaca serpentine; J, jadeite; Q, green quartz.

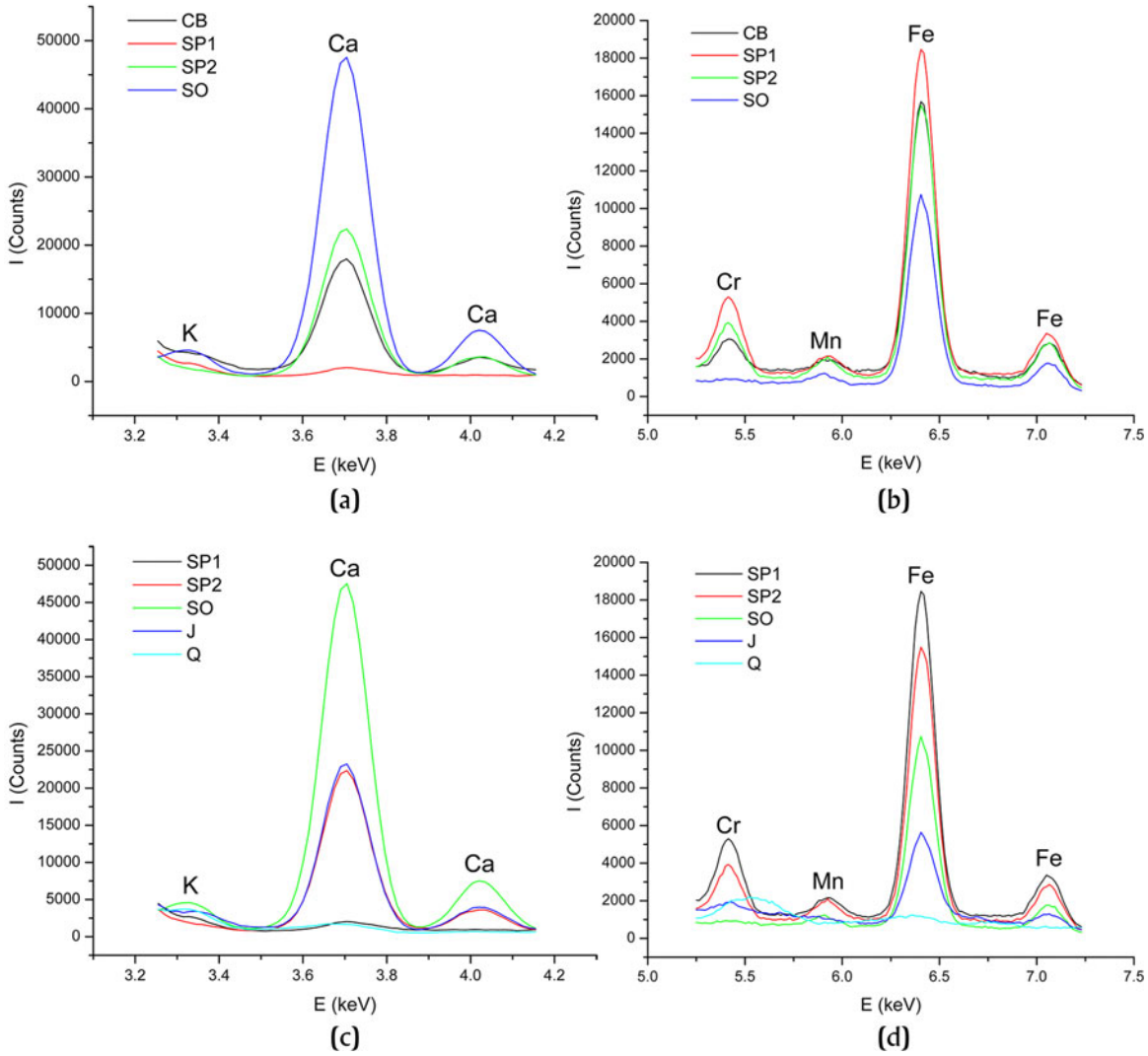

Figure 11. Portable dispersive energy X-ray fluorescence spectrometry spectra corresponding to the Light stage of irradiation. CB, Cascajal Block; SPl and SP2, Puebla serpentine; SO, Oaxaca serpentine; J, jadeite; Q, green quartz.

https://doi.org/10.1017/S0956536119000257 Published online by Cambridge University Press

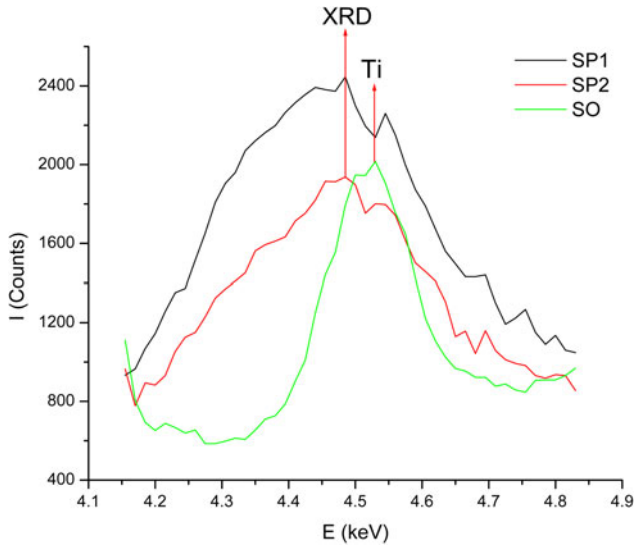

Figure 12. Portable dispersive energy X-ray fluorescence spectrometry spectra corresponding to the Light stage of irradiation of the chemical signatures of the serpentine samples (SPI and SP2, Puebla serpentine; SO, Oaxaca serpentine), in which the presence of an X-ray diffraction (XRD) signal is noted at 4.47 KeV in the Puebla serpentine spectra.

If the CB is, in fact, Tehuitzingo serpentine, then we should expect to encounter the diffraction signal described above—and noted in the samples—in the pXRF spectra of the object. In the Light irradiation stage spectra (Figure 13), just such a signal is detected at 4.47 keV, associated with the interplanar distance of 1.52 Å. This is identical to the peak observed in the spectra of the Tehuitzingo serpentine (SP1 and SP2 in Figure 12), but not in the Oaxaca serpentine (SPO in Figure 12) or additional greenstone samples (Q and J in Figure 13). In conjunction with the qualitative pXRF data discussed above, this diffractometric spectral identification provides further data to establish definitively that the constituent material of the CB is serpentine, and supports the hypothesis that its source is the Tehuitzingo deposit in Puebla.

Patination Patterns and Contextual Information Revealed in the pXRF Data

A second set of anomalous readings appeared in the Light stage pXRF spectra. In these, potentially significant differences between the peak intensities of the Si and Mg signals are evident in the CB spectrum with respect to those of the serpentine reference samples (Figure 14). Due to the low Si and Mg readings for the CB matrix revealed in the pXRF spectra, we turned to the results of the quantitative chemical analysis (Table 1) to determine the mass concentrations of those elements present on the CB. Focusing for the moment on Si, the quantitative data show that, in terms of the interaction volume (in which the primary X-ray beam is completely attenuated), Si is found in mass concentrations between 1.26 ppm and 1.72 ppm. These values are somewhat unusual for the chemical composition of a lithic matrix, but may be attributable to the mineral qualities of serpentine. Since the Pearson Coefficient of Variation (CV) is less than 15 percent, we may conclude that the low concentration of Si on the surface of the CB is a generalized condition. Likewise, the unquantifiable fraction of the lithic matrix exceeds 90 percent, with a similarly low CV value (0.42 percent), which again suggests a generalized condition for the CB surface. Together, these data suggest the presence of a uniform patina on the CB surface, contrary to the variable patina apparently evident via visual examination and reported by Rodríguez Martínez et al. (2006:1612).

This patina could have formed through two geochemical processes. First, it is possible that the chemical-compositional characteristics are a consequence of the generalized presence on the CB surface of a mineral patina produced by authigenesis, a process whereby a mineral deposit (such as a patina) is generated where it is found or observed (Pérez Jiménez 2010:238–242; Ritger et al. 1987; Ruttenberg and Berner 1993), which would hinder the

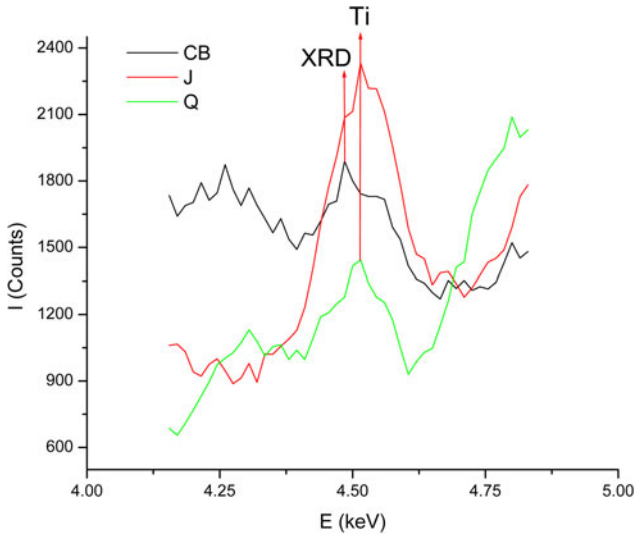

Figure 13. Portable dispersive energy X-ray fluorescence spectrometry spectra corresponding to the Light stage of irradiation of the chemical signatures of the Cascajal Block (CB) and additional greenstone samples (J, jadeite; Q, green quartz), in which the presence of an X-ray diffraction (XRD) signal is noted at 4.47 KeV in the CB spectrum.

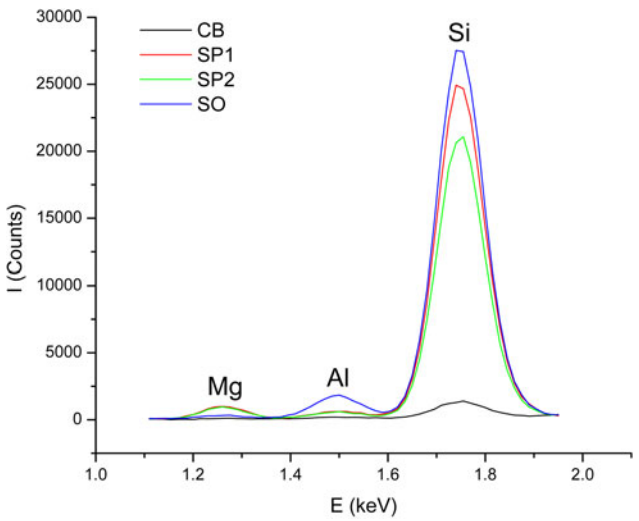

Figure 14. Portable dispersive energy X-ray fluorescence spectrometry spectra corresponding to the Light stage of irradiation of the chemical signatures of the Cascajal Block (CB) and serpentine samples (SPI and SP2, Puebla serpentine; SO, Oaxaca serpentine).

https://doi.org/10.1017/S0956536119000257 Published online by Cambridge University Press

Table 1. Results of the quantitative chemical analysis of Cascajal Block (CB) surfaces. NQ, part of the matrix that could not be quantified; CV, Pearson Coefficient of Variation.

Visual ID[a]	Sampled Surface[b]	NQ % ± σ %	Si % ± σ %	Fe % ± σ %	Cr % ± σ %
Apparently unpatinated	CB1	91.29 ± 0.03	1.41 ± 0.02	5.82 ± 0.03	0.163 ± 0.002
Apparently unpatinated	CB2	91.62 ± 0.17	1.42 ± 0.04	5.70 ± 0.19	0.170 ± 0.007
Apparently unpatinated	CB3	91.87 ± 0.03	1.36 ± 0.02	5.45 ± 0.03	0.215 ± 0.002
Light blue patina	CB4	91.45 ± 0.03	1.26 ± 0.02	5.57 ± 0.03	0.175 ± 0.002
Apparently unpatinated	CB5	91.10 ± 0.03	1.72 ± 0.02	5.57 ± 0.03	0.195 ± 0.002
Apparently unpatinated	CB6	92.27 ± 0.03	1.11 ± 0.02	5.48 ± 0.03	0.193 ± 0.002
Yellowish deposit	CB7	91.71 ± 0.03	1.32 ± 0.02	5.62 ± 0.03	0.166 ± 0.006
Light blue patina	CB8	91.26 ± 0.03	1.32 ± 0.02	6.12 ± 0.03	0.204 ± 0.002
	CV %	0.42	12.58	3.86	10.266
Visual ID	Sampled Surface	Mn ppm ± σ ppm	Mg ppm ± σ ppm		
Apparently unpatinated	CB1	822.85 ± 40.90	0.00 ± 0.00		
Apparently unpatinated	CB2	782.69 ± 42.91	0.00 ± 0.00		
Apparently unpatinated	CB3	709.65 ± 36.76	0.00 ± 0.00		
Light blue patina	CB4	718.91 ± 37.62	0.00 ± 0.00		
Apparently unpatinated	CB5	765.15 ± 38.57	0.00 ± 0.00		
Apparently unpatinated	CB6	818.61 ± 38.86	0.00 ± 0.00		
Yellowish deposit	CB7	802.76 ± 43.32	0.00 ± 0.00		
Light blue patina	CB8	763.78 ± 38.60	0.00 ± 0.00		
	CV %	5.50			

[a]Sample areas were selected on the basis of visual inspection, to include both patinated and (apparently) unpatinated areas (although subsequent analysis indicated uniform patina).
[b]See Online Appendix 1.

correct quantification of light chemical elements such as Si or Mg (due to the attenuation of the primary beam in the volume of the patina, which would cause considerable difficulties for the quantification of other chemical elements). If the patina was produced authigenetically, however, the CB would present a greater set of inconsistencies with the serpentine samples. But this is not the case. Rather, the mass concentrations of Fe, Cr, and Mn in the CB are consistent with the samples—evident in the Kα and Kβ signal intensities in the corresponding pXRF spectra (Figures 8–11), as well as in the quantitative data (Table 2). Comparing these data suggests Si and Mg are outliers in the CB spectra, since all other elemental determinations display strong similarities between the CB composition and the diagnostic chemical signatures of the (unpatinated) serpentine samples (% and ppm of Cr, Mn, and Fe in Table 2). As an aside, it is noteworthy that the quantitative chemical data in Table 2 also suggest stronger correspondences between the CB and the Tehuitzingo serpentine samples, and differences with the sample from Oaxaca (particularly in terms of Cr percentage), further supporting the identification of the Tehuitzingo deposit as the source of the CB serpentine.

Table 2. Results of the quantitative chemical analysis of the Cascajal Block (CB) and the serpentine mineral samples. SP1 and SP2, Puebla serpentine; SO, Oaxaca serpentine; NQ, part of the matrix that could not be quantified.

Sample	NQ (%) ± σ (%)	Si (%) ± σ (%)	Mg (%) ± σ (%)
CB	91.57 ± 0.04	1.36 ± 0.02	0.00 ± 0.00
SP1	62.70 ± 0.07	21.15 ± 0.07	8.86 ± 0.11
SP2	60.57 ± 0.08	21.50 ± 0.07	8.70 ± 0.12
SO	41.06 ± 0.10	34.79 ± 0.11	4.12 ± 0.14
Sample	Cr (%) ± σ (%)	Mn (ppm) ± σ (ppm)	Fe (%) ± σ %
CB	0.185 ± 0.003	773.05 ± 39.69	5.67 ± 0.05
SP1	0.481 ± 0.002	675.55 ± 24.70	5.19 ± 0.02
SP2	0.328 ± 0.002	865.88 ± 26.12	5.53 ± 0.02
SO	0.000 ± 0.000	1,514.28 ± 31.55	6.23 ± 0.02

It is more likely that these anomalous results are due to a patina produced via a superficial erosion process, through which the mass concentration of Si on all surfaces of the CB decreased significantly, to a level below two percent (Tables 1 and 2). A similar process may be surmised for Mg. In the case of serpentine, Krevor and Lackner (2011) have reported that these chemical characteristics—low levels of Si and Mg in mineral surface accumulations—are the result of the geochemical process of dissolution. In dissolution, hydrolysis of the surface crystalline structure occurs, with a consequent loss of SiO_2 and an accumulation of magnesium carbonate on the surface, via the following chemical reactions:

$$\tfrac{1}{3}Mg_3Si_2O_5(OH)_4 + 2H^+ \rightarrow Mg^{2+} + \tfrac{2}{3}SiO_2(aq) + \tfrac{2}{3}H_2O$$

$$Mg^{2+} + HCO_3^- \rightarrow MgCO_3(s) + H^+$$

This process particularly affects serpentine in humid, acidic soils. Sanna et al. (2017) report that these reactions are accelerated in environments with high concentrations of sodium salts, which subsequently replace Si on the surface. The resulting accumulations of magnesium carbonate on the surface, however, tend to dissolve in these humid, saline contexts. In constant conditions, the process culminates with the establishment of a solid-liquid phase equilibrium after approximately six hours of contact (Dong et al. 2009).

Of course, an archaeological context is a dynamic system in which conditions are rarely constant. In sealed contexts, a buried object will never be in contact with a constant volume of liquid, since soil humidity is dependent on variable hydrographic

https://doi.org/10.1017/S0956536119000257 Published online by Cambridge University Press

characteristics and levels of rainfall in a given region. Thus, in real-world conditions distinct from the ideals established by Dong et al. (2009), phase equilibrium is difficult to achieve, much less in a question of hours. Accordingly, dissolution of Si and (subsequently) magnesium carbonate and the consequent surface deposition of sodium salts is a long-term, continuous process, influenced by factors such as variability between the exchange rate and dissolution coefficient, ambient temperature, soil pH, and concentration of salts in the liquid phase (Dong et al. 2009), particularly $MgCl_2$, since increased levels of this saline compound accelerate the dissolution of magnesium carbonate from the solid phase (Sanna et al. 2017).

The simultaneous processes of dissolution of a serpentine matrix and dissolution of superficial magnesium carbonate may provide a window onto the depositional contexts and dating of a serpentine object that displays surface erosion and low levels of Mg. Konrad et al. (2018) report that the dissolution of serpentine takes between 10^3 and 10^5 years. We would thus expect that extended burial of a serpentine object in specific soil conditions would lead to surface erosion via dissolution. Dissolution, in turn, would result in the formation of a uniform patina that would display low mass concentrations of Si and Mg in spectrometric analyses, due to the continuous dissolution of the magnesium carbonate produced in the process of serpentine dissolution, which itself would be replaced by the deposition of sodium salts on the surface.

Our results reflect precisely such characteristics on the CB. The chemical determination of Mg in the CB matrix did not yield quantifiable results, whereas Mg is evident in the three other samples of serpentine (Tables 1 and 2). Further, the pXRF spectra corresponding to the Light stage of irradiation (Figure 14) also reflect this discrepancy and display significant differences between the intensities of the Kα signals of both Si and Mg for the CB relative to the serpentine samples. It is possible that uneven distribution of superficial sodium salts is responsible for what appears visually to be variable patina on the CB.

Since Mg is a fundamental element in the chemical composition of serpentine, its relatively low concentrations on the CB are most likely due to the specific edaphological characteristics of the context of its original deposition, which resulted in the dissolution process that yielded the specific chemical signatures of the object. The context reported for the discovery of the CB (Rodríguez Martínez and Ortiz Ceballos 1999, 2007; Rodríguez Martínez et al. 2006) is a riverine environment in which high humidity luvisols with an albic horizon predominate (INEGI 2019; López et al. 2011:23). The average pH of these luvisols is slightly acidic, between 5 and 6 (Campos Cascaredo 2011). Further, several salt domes are concentrated in the area (Benavides García 1983), resulting in high levels of soil salinity. Thus, the soil conditions of the immediate area in which the CB was found are ideal for the geochemical process of dissolution to occur and produce precisely the chemical signatures evident in the CB spectra. The albic horizon reported for soils in the region is also significant in this regard, since it would cause a considerable deficit of Fe in the subsoil. Such conditions would impede excessive enrichment of the CB surface with this element, thereby explicating the similar peak intensities for Fe between the CB and the unpatinated serpentine samples.

The anomalous readings for Si and Mg revealed in the Light irradiation XRF analysis of the CB matrix thus have led, fortuitously, to three key inferences. First, these readings indicate the presence a generalized mineral condition on the CB surface, that is, a uniform patina. Although it is true that patina can be artificially induced, the presence of patination on the entirety of the CB surface—including directly on top of the incised signs—is an excellent indicator of the object's antiquity. Second, the dissolution processes that led to the formation of this patina also attest to the age of the object, in terms of the temporal context of its deposition. Since the *terminus ante quem* for which the process of dissolution of the CB serpentine began is at least 10^3 years (Konrad et al. 2018), we can confidently conclude that the object is pre-Hispanic in origin. Finally, dissolution that would result in the specific chemical characteristics evident in the CB can only occur in specific edaphological environments—conditions which align precisely with the humid, slightly acidic, saline soils common in southeast Veracruz. The most parsimonious explanation for these data is therefore that the original depositional context of the object was indeed the context in which it was reported to have been found (Rodríguez Martínez and Ortiz Ceballos 1999, 2007; Rodríguez Martínez et al. 2006). Taken as a whole, the data derived from pXRF analysis of the CB strongly support the authenticity of the object.

ANALYSIS OF MANUFACTURING TRACES: COMPARATIVE EVALUATION OF INCISION MICROSTRUCTURE VIA SEM

Determinations of cultural affiliation and temporal context are particularly difficult for objects that, like the CB, lack secure archaeological contexts. The absence of such contexts may lead to doubts regarding an object's authenticity, a frequent critique of the CB (e.g., Bruhns et al. 2007; Cyphers 2007). The traceological analysis of marks left by the materials employed in an artifact's manufacture is a method commonly used to recover part of this missing contextual information (Li et al. 2011; Sax et al. 2004) and also assists in evaluating an object's authenticity (Walsh 2008). In this case, we used SEM to analyze manufacturing traces evident in the CB's incised text via the comparative analysis of incision microstructure revealed through SEM micrographs of polymer replica molds against manufacturing traces evident on experimentally produced reference specimens and a selection of Formative-period artifacts of known archaeological context or recognized authenticity.

We first created polymer replicas that duplicated the microstructure of incisions on the CB. Replicas were created by softening a 25 mm^2 cut piece of Buehler replicating tape with acetone, which was then pressed against the object surface for approximately one minute (Figure 15) and removed with surgical tweezers. Fifteen areas were sampled on the CB (including sides and uninscribed areas; Online Appendix 2). For redundancy, four molds were created for each sampled surface. The replicas were then placed into prelabeled 55 × 76-mm polythene bags and transported to the Instituto Nacional de Antropología e Historia's (INAH) Museo del Templo Mayor (MTM) in Mexico City. Polymer replicas were compared with the naked eye, with the aid of a magnifying loupe at 20 × magnification, and with a Leica MZ6 stereoscopic microscope at 10 × and 30 × magnification. Optic microscopy revealed various diffuse and heavily textured lines within the incision replicas.

The polymer replicas were subsequently covered with gold ions for observation in a JEOL JSM 6460LV scanning electron microscope housed in INAH's Laboratorio de Microscopía Electrónica. Samples were observed in High Vacuum mode, which allows the best resolution, at 100×, 300×, 600×, and 1000 × magnification, under constant parameters (Secondary Electron Imaging, spot size = 49, distance = 10 mm, voltage = 20 kV). The highest

https://doi.org/10.1017/S0956536119000257 Published online by Cambridge University Press

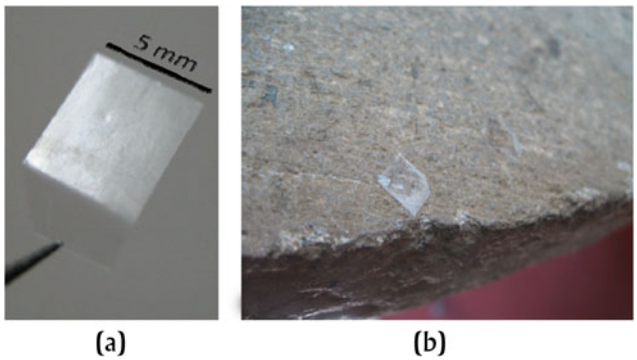

Figure 15. Creating polymer replica molds. (a) Replicating tape. (b) Application on object surface to duplicate microstructure and obtain manufacturing traces.

magnification level offers the most precise results, and is ideal for characterizing superficial microstructural traits such as manufacturing traces. Using this particular SEM's Microscope Image Capture System, micrographs of surface microstructure of the CB incisions were created (Figure 16).

In these, we observe characteristics such as the direction and size of bands and lines, as well as their roughness and texture. The most salient data revealed through SEM analysis that speaks to manufacture is the presence of fine, irregular, and diffuse lines of between 0.6 and 1.3 μm in width in the inscriptions. All samples were analyzed, and these characteristics were noted in all of the samples pertaining to inscribed areas (Figure 16 is thus an exemplar of a general trend). The exceptions were the "null" samples of uninscribed areas on the block (10 and 11; see Online Appendix 2). In these cases, traces of diffuse bands of 10 μm in width, as well as fine lines of 3.5 μm in width, are evident (Figure 17). These are the same marks noted in the CB PTM (Figure 6). These characteristics were then compared with those evident on Formative-period archaeological objects of known provenience and reference specimens produced through experimental archaeology that were analyzed following the same methodology described above.

Comparative Analysis

The comparative pieces reported here were selected from the collections of the Universidad Veracruzana's Museo de Antropología de Xalapa (MAX, https://www.uv.mx/max), which houses one of the largest collections of Olmec art in the world. Although, as is the case with many Olmec objects, not all of the archaeologically known reference specimens come from controlled excavations with radiocarbon dating, INAH and international specialists have previously verified the authenticity of all of the reference specimens employed here as part of the incorporation of these objects into INAH's Registro Público Nacional de Monumentos y Zonas Arqueológicos e Históricos. We have focused on those objects that do have secure provenience and were recovered from systematic excavation or have reliable dates, such as La Mojarra Stela 1 and the jadeite object, greenstone celts, and figurines from Arroyo Pesquero, Veracruz (Wendt et al. 2014; Winfield Capitaine 1988). The archaeological contexts and cultural affiliations of the comparative reference sample are therefore secure. The CB samples were evaluated against micrographs of the surface structure of modifications on over 70 Olmec stone objects in the MAX (and other) collections that were previously analyzed with the methodology employed here (Bernard and Melgar Tísoc 2016, 2018; Bernard et al. 2018; Solís Ciriaco et al. 2016).

Samples were also compared against experimentally produced reference specimens created at INAH MTM's Experimental Archaeology and Lapidary Workshop. Since 2005, the workshop has employed experimental techniques to characterize the traces left by distinct manufacturing techniques used to produce ancient Mesoamerican lapidary objects (Melgar Tísoc 2017; Melgar Tísoc and Solís Ciriaco 2005, 2009, 2015, 2018). Since artifacts are fabricated and used in accordance with culturally specific criteria and schemes, the manufacturing process(es) used to create them leave characteristic traits (Andrefsky 2006; Ascher 1961; Braun et al. 2008; Eren et al. 2016; Laughlin y Kelly 2010; Lerner 2013; Marsh and Ferguson 2010; McPherron et al. 2014; Nami 2010; Putt 2015). The workshop seeks to replicate distinct types of modifications evident on archaeological objects, such as cuts, reductions, incisions, perforations, fretwork, and finishes (Melgar Tísoc 2017:120, Figure 1; Melgar Tísoc and Solís Ciriaco 2009: 120, Figure 2, 2015:122, Figure 4, 2017:268, Figure 18.1, 2018: 646, Figure 19.22; Melgar Tísoc et al. 2012:107, Figure 7; Monterrosa Desruelles and Melgar Tísoc 2017:915, Figure 6). It does so by using tools and materials available to pre-Hispanic groups, as identified in historical sources or in the archaeological record (Charlton 1993; Durán 1967; Feinman and Nicholas 1995; Mirambell 1968; Moholy-Nagy 1997; Sahagún 1956). To date, the workshop's reference collection encompasses 520 objects,

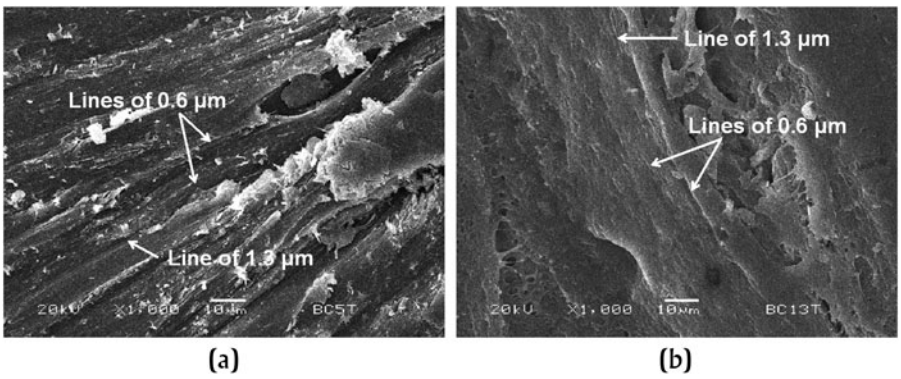

Figure 16. Micrographs of surface microstructure taken from the Cascajal Block incised text: (a) Sample 5 and (b) Sample 13.

https://doi.org/10.1017/S0956536119000257 Published online by Cambridge University Press

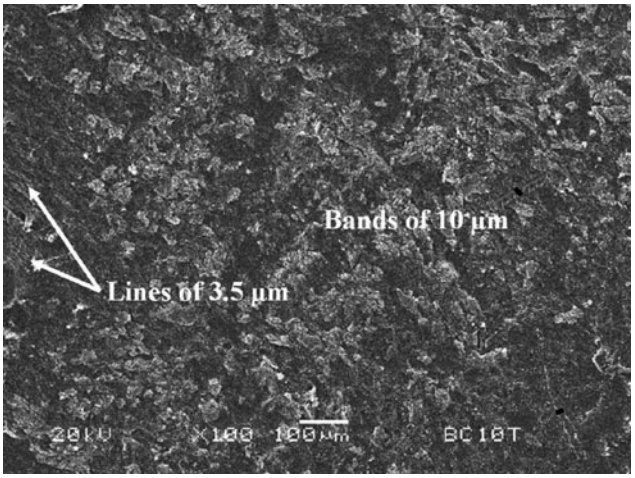

Figure 17. Micrograph of surface microstructure in an uninscribed area of the Cascajal Block (Sample 10).

produced with a variety of pre-Colombian lithic techniques, as well as modern tools, on various media.

In traceological analyses, features noted on reference specimens experimentally elaborated may be used to determine the techniques employed in the manufacture of archaeological materials. This is possible since the elaboration and use of lapidary objects produced under similar conditions and with the same techniques will leave characteristic patterns and differentiable features that can be compared against archaeological objects. Following interpretive criteria developed for the study of shell artifacts (Velázquez Castro 2007) and adjusted to lapidary objects, the workshop has identified the tools, materials, and processes most commonly employed in the manufacture of Mesoamerican lapidary objects (Table 3). Further, the workshop has identified several particular regional and temporal styles that characterize the lapidary production technologies of various Mesoamerican cultural groups, including Aztec (Melgar Tísoc and Solís Ciriaco 2009, 2015, 2017; Solís Ciriaco and Melgar Tísoc 2017), Mixtec (Melgar Tísoc and Solís Ciriaco 2017), Zapotec (Melgar Tísoc et al. 2010), Teotihuacano (Melgar Tísoc 2017; Melgar Tísoc and Solís Ciriaco 2018; Melgar Tísoc et al. 2018), Maya (Melgar Tísoc 2017; Monterrosa Desruelles and Melgar Tísoc 2017; Solís et al. 2016), and Olmec (Bernard and Melgar Tísoc 2016, 2018; Bernard et al. 2018; Melgar Tísoc et al. 2018; Monterrosa Desruelles and Melgar Tísoc 2017; Solís Ciriaco et al. 2016), among others. These characterizations assist in the determination of cultural affiliations and temporal contexts for unprovenienced materials, since discrete cultures employed distinct lapidary toolkits at different points in time, which leave particular manufacturing traces on the objects.

Table 3. Types of lithic modification and the tools and materials employed to create them.

Modification	Materials Employed
Reduction and abrasion	Basalt, andesite, rhyolite, sandstone, limestone, granite, slate, and jade; adding water and (occasionally) sand.
Cuts	Sand or volcanic ash, water, and strips of hide or vegetal fibers. Flint and obsidian tools; petrified wood.
Perforations	Abrasives (sand, volcanic ash, obsidian dust, flint dust, quartz dust), with large diameter reed branches and water. Flint, quartz, and obsidian tools; petrified wood.
Fretwork	Abrasives (sand, volcanic ash, obsidian dust, flint dust, quartz dust), with large diameter reed branches and water.
Incisions	Flint and obsidian tools; petrified wood.
Finishes	Polished with abrasives, water, and hide, or with jade, flint, and corundum. Dry burnished with hide and a combination of abrasives and water.

For the purposes of this study, experimental reductions and incisions on Tehuitzingo serpentine—the same used for the pXRF analyses described above—were made with numerous abrasives and sharp-edged lithic tools, including flint flakes and obsidian blades, as well as chert, sandstone, limestone, andesite, and quartz. Sharp-edged tools were employed in this case since instruments with retouched edges leave thicker and coarser traces, which differ from the fine, superficial features evident on the CB. Polymer replica molds were created of these incisions and abrasions, following the methodology outlined above, then subjected to SEM analysis under the same parameters, and finally compared to micrographs of the CB samples. Micrographs of experimental pieces and CB samples were also compared against those of reference specimens from other lapidary traditions on multiple media (see, e.g., Melgar Tísoc 2017:122–123, Figures 5–10; Melgar Tísoc and Solís Ciriaco 2017:274–279, Figures 18.5–18.9; Melgar Tísoc et al. 2012:111, Figures 12–14), including serpentine, jadeite, quartz, and other greenstones commonly worked by Olmec groups (cf. Melgar Tísoc and Solís Ciriaco 2018:649–653, Figures 19.25–19.30). Thus, a large, diverse reference sample was employed to serve as the baseline against which the manufacturing traces on the CB were compared.

The fine, irregular, and diffuse lines of between 0.6 and 1.3 µm in width on the CB's inscribed surface revealed via SEM analysis (Figures 16, 18a, and 18b) are similar to those experimentally produced by obsidian tools (Figure 18c; see also Melgar Tísoc 2017:122, Figure 7; Melgar Tísoc and Solís Ciriaco 2015:124, Figure 6a, 2017:279, Figure 18.6, 2018:653, Figure 19.26) and distinct from those left by other materials, such as flint (Figure 18d; see also Melgar Tísoc and Solís Ciriaco 2018:650, Figure 19.26), chert (Melgar Tísoc 2017:122, Figure 8; Melgar Tísoc and Solís Ciriaco 2015:124, Figure 6d), modern tools (Melgar Tísoc and Solís Ciriaco 2009:Figures 11 and 12; Walsh 2008:Figures 6–8), and other materials (Melgar Tísoc and Solís Ciriaco 2009:Figures 6–13; Melgar Tísoc and Solís Ciriaco 2015:Figures 5–7). Comparing manufacturing traces on the CB incisions to those evident in archaeologically known incised materials from the Olmec nuclear area of the Gulf Coast (Figure 19), the patterns coincide. Several incised objects of Formative-period Olmec origin in the MAX collections, for example, previously analyzed with the methodology employed here (e.g., Bernard and Melgar Tísoc 2016, 2018; Bernard et al. 2018), present identical manufacturing traces, with fine, irregular, and diffuse lines of the same width as those observed in the CB incisions. These include Las Limas Monument 1, an incised serpentine object from Jesús Carranza, Veracruz (Figure 19a); a greenstone celt from Arroyo Pesquero, Veracruz (Figure 19b); a jadeite object from Arroyo Pesquero (Figures 19c and 19d; Wendt et al. 2014); a greenstone figurine also from Arroyo Pesquero (Figure 19e); and the

https://doi.org/10.1017/S0956536119000257 Published online by Cambridge University Press

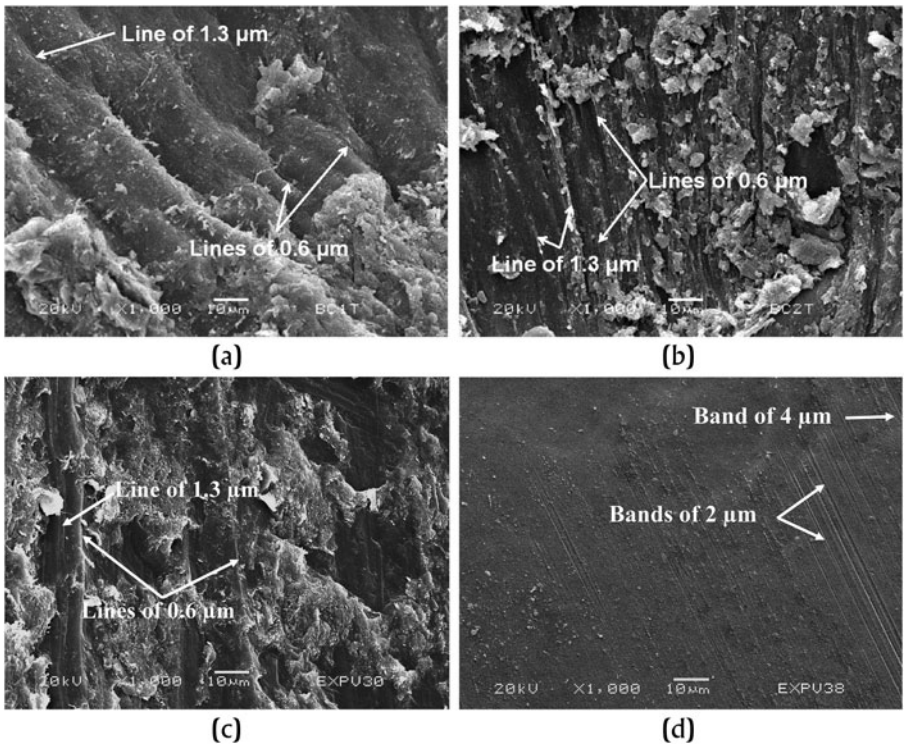

Figure 18. Comparative micrographs of Cascajal Block (CB) incisions and experimental manufacturing traces. (a) CB Sample 1. (b) CB Sample 2. (c) Experimental obsidian-on-serpentine incision. (d) Experimental flint-on-serpentine incision.

incised text of La Mojarra Stela 1 (Figure 19f; Winfield Capitaine 1988).

In the case of the unincised surfaces, the diffuse 10 µm bands and fine 3.5-µm lines noted on the CB (Figures 17 and 20a) are identical to those produced by the experimental abrasion of serpentine with sandstone (Figure 20b; see also Monterrosa Desruelles and Melgar Tísoc 2017:915, Figure 7d). Such traces have also been identified on several Olmec objects of secure Middle Formative-period contexts at sites such as Arroyo Pesquero, San Lorenzo, La Venta, and Loma del Zapote (Bernard and Melgar Tísoc 2018), in objects from the MAX collections such as Las Limas Monument 1 (Figure 20c; Bernard et al. 2018), and even in objects from further afield, such as the incised celt with Olmec iconography from Chiapa de Corzo, Chiapas (Figure 20d; Solís Ciriaco et al. 2016). These patterns likewise differ significantly from those left by other reduction techniques characterized in previous experimental and traceological work, such as abrasion with basalt (Melgar Tísoc and Solís Ciriaco 2017:274, Figure 18.5, 2018:654, Figure 19.31; Melgar Tísoc et al. 2012:11, Figure 12b), andesite (Melgar Tísoc 2017:122, Figure 6; Melgar Tísoc and Solís Ciriaco 2018:649, Figure 19.25; Monterrosa Desruelles and Melgar Tísoc 2017:915, Figures 7b and 7c), or limestone (Melgar Tísoc 2017:122, Figure 5; Melgar Tísoc and Solís Ciriaco 2018: 652, Figure 19.28; Melgar Tísoc et al. 2012:111, Figure 14b).

The manufacturing traces evident on the CB and Olmec materials of known provenience thus coincide, suggesting that the CB incisions were made with sharpened obsidian tools and that surface reduction was realized via abrasion with sandstone, both common instruments and techniques in the pre-Hispanic lapidary toolkit. Although some of these reference specimens are comprised of materials others than the serpentine that constitutes the CB (e.g., jadeite [Figure 18c and 18d] or greenstone [Figures 18b, 18e, and 19d]), the same manufacturing traces are evident on all experimental and control reference specimens. Previous studies (Bernard and Melgar Tísoc 2016, 2018; Bernard et al. 2018; Melgar et al. 2018; Monterrosa Desruelles and Melgar Tísoc 2017; Solís Ciriaco et al. 2016) suggest that Olmec lapidary technology is characterized in part by obsidian incision and sandstone abrasion, which differs from techniques evidenced in lithic artifacts produced by other Mesoamerican cultural groups (Melgar Tísoc 2017; Melgar Tísoc and Solís Ciriaco 2015, 2017, 2018; Melgar et al. 2010, 2018; Monterrosa Desruelles and Melgar Tísoc 2017; Solís Ciriaco and Melgar Tísoc 2017). Finally, Monterrosa Desruelles and Melgar Tísoc (2017; see also Melgar Tísoc 2017) argue that these patterns are diagnostic of a specific temporal context, in which manufacturing techniques were standardized sometime prior to the Middle-to-Late Formative-period transition (ca. 700–500 B.C.), after which greater variability is evident in Olmec lapidary industries. We thus conclude that, from a technological standpoint, the CB was fabricated using the same lapidary technologies characteristic of the Early and Middle Formative periods evident on other Olmec objects of known contexts or recognized authenticity. These results therefore support interpretations of the CB as a product of the Olmec culture and bolster claims for its dating, further arguing for its authenticity. Finally, this research adds additional data that advances scholarly understanding of the lapidary technologies employed during the Middle Formative period, particularly among Olmec cultural groups.

https://doi.org/10.1017/S0956536119000257 Published online by Cambridge University Press

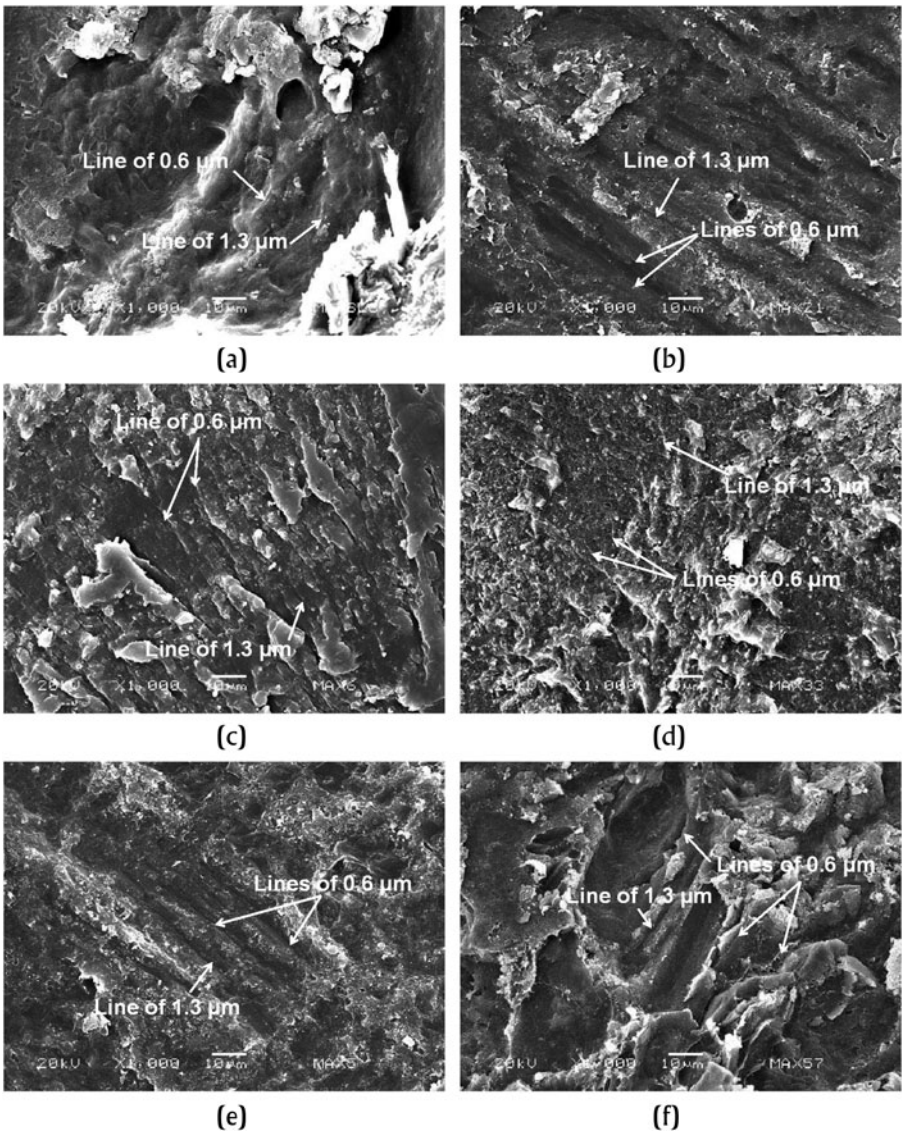

Figure 19. Comparative micrographs of manufacturing traces on Olmec materials of known contexts. (a) Incision on Las Limas Monument 1. (b) Incision on a greenstone celt from Arroyo Pesquero. (c and d) Incisions on a mottled brown and white jadeite object from Arroyo Pesquero. (e) Incision on a greenstone figurine from Arroyo Pesquero. (f) Incision from text on La Mojarra Stela 1.

CONCLUSIONS

Results of the analyses reported here corroborate previous interpretations of the CB as an authentic object affiliated with the Formative-period Olmec culture. High-resolution examination of the CB surface and its incised text via PTM revealed marks that may suggest earlier inscriptional strata, as well as variable wear and weathering patterns that could indicate possible erasure, supporting previous hypotheses (Rodríguez Martínez et al. 2006:1612). In addition, these marks may provide clues as to the function of the object after it was inscribed. These results are not, however, definitive. We are planning further analyses of the object's surface following the methodologies employed in this study, including mineralogical analyses and comparative evaluation of possible palimpsest incisions against known standards, to address these issues more conclusively.

PTM imagery, however, assisted considerably in refining details difficult to observe via conventional photography or visual examination, in terms of identifying previously unpublished aspects in the inscribed text. With this new data, we created a new epigraphic drawing of the CB text that more accurately identified specific signs. The proper identification of incised motifs is crucial to advancing scholarly understanding of singular texts, such as that on the CB, and generating new hypotheses to drive future research. The conclusive identification of additional Middle Formative-period motifs in the CB text that correspond to contemporaneous Olmec iconographic canons (see also Carrasco and Englehardt 2015:640) circumstantially supports the object's dating and cultural affiliation, and serves to complement the inferences derived from the archaeometric analyses we realized.

Qualitative and quantitative spectrometric analysis via pXRF revealed a strong similarity between the chemical signatures for the CB and serpentine, particularly samples of that mineral from the Tehuitzingo, Puebla deposit, a common source of serpentine

https://doi.org/10.1017/S0956536119000257 Published online by Cambridge University Press

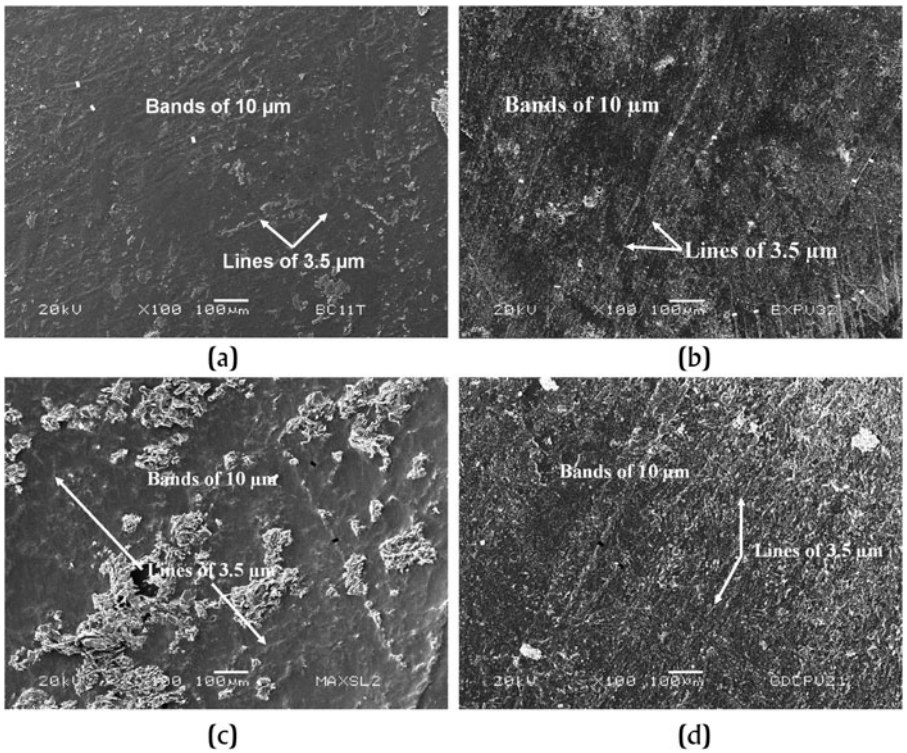

Figure 20. Comparative micrographs of reduction and abrasion on unincised areas of the Cascajal Block (CB), experimental manufacturing traces, and reduction traces on Olmec materials of known contexts. (a) CB Sample II. (b) Experimental abrasion of sandstone on serpentine. (c) Las Limas Monument 1. (d) An incised greenstone celt with Olmec iconography from Chiapa de Corzo.

used in Middle Formative-period objects (Robles Camacho et al. 2008). Affiliation with the Tehuitzingo deposit was also suggested by superficial visual comparison of coloring and patination patterns evident on both the CB and other objects manufactured with Tehuitzingo serpentine. An XRD signal detected in the pXRF spectra also supports the identification of the CB material matrix as serpentine and further links the CB serpentine to the Puebla source. Our results thus confirm the previous identification of the material as serpentine, and we conclude that the most likely source of the CB serpentine is Tehuitzingo, Puebla. Additional multielemental chemical analyses of mineral samples from this and other serpentine deposits are currently planned to further evaluate this inference.

Serpentine is a somewhat unusual medium for an inscribed text (Bruhns et al. 2007:1365) and we know of no other Olmec serpentine object with similar incisions, with the possible exception of Las Limas Monument 1. Nevertheless, shallow line incisions in other greenstone media are relatively common (Winfield Capitaine 1988) and serpentine was often used in Olmec sculptural and ritual contexts, for example, in the serpentine blocks recovered from the massive offerings at La Venta Complex A (Drucker 1952; Drucker et al. 1959) that are nearly identical to the CB in size and shape. Why this inscription was carved in a large block of serpentine that could otherwise have been used to craft hundreds of beads or dozens of figurines is unknown. This and other questions cannot be resolved until further examples of the CB script or incised serpentine objects affiliated with the Olmec culture are found.

Anomalous readings for the elements Si and Mg in the CB pXRF spectra unexpectedly provided strong evidence that speaks to the antiquity and depositional contexts of the object. A uniform patina was identified, based on quantitative differences between the elemental mass concentrations of these elements in the CB matrix relative to the serpentine reference samples. The presence of a generalized mineral patina on the entirety of the CB surface is an excellent indicator of the object's antiquity. In turn, we deduced that the chemical characteristics that resulted in these anomalous Si and Mg readings could only have been caused by the geochemical process of dissolution, a formation process that takes at least 1,000 years (Konrad et al. 2018). In addition, dissolution of serpentine that would result in the precise chemical signatures detected in our analysis only occurs in very specific edaphological and geochemical environments, namely humid, slightly acidic luvisols that present high ambient salinity and an albic horizon. These conditions match those reported for the context of the CB (Rodríguez Martínez and Ortiz Ceballos 1999, 2007; Rodríguez Martínez et al. 2006). The most logical conclusion suggested by these data is that the CB was deposited and buried for an extended period in the context in which it was reportedly encountered. The XRF analysis therefore provided further authenticating data that strongly suggest the object's origins in the Formative period of southeastern Veracruz, as well as suggesting a source of the CB serpentine in the Tehuitzingo deposit.

Finally, traceological analysis of surface microstructure via SEM of polymer replica molds taken from incised and uninscribed areas on the CB revealed particular manufacturing traces. These include the presence of fine, irregular, and diffuse lines of between 0.6 and 1.3 µm in width in the inscriptions, and diffuse bands of 10 µm in width and fine lines of 3.5 µm in width on unincised surfaces. Systematic comparative analysis of these characteristics against micrographs of manufacturing traces on experimentally produced

https://doi.org/10.1017/S0956536119000257 Published online by Cambridge University Press

reference specimens and archaeological objects of known provenience from various cultural traditions revealed high degrees of consistency between the CB tool marks and those from securely contextualized inscribed Olmec objects. Further, these manufacturing traces are diagnostic of a specific temporal context, prior to the Middle-to-Late Formative-period transition, in which lapidary techniques were standardized across Olmec cultural groups (Melgar Tísoc 2017; Monterrosa Desruelles and Melgar Tísoc 2017). This experimental verification thus leads us to conclude that the manufacturing traces on the CB are the result of its fabrication using pre-Hispanic tools and techniques indicative of Olmec lapidary industries prior to ca. 700–500 B.C. These results further authenticate the object and support interpretations of the CB as an Olmec artifact of Middle Formative-period manufacture.

In sum, although the CB is a unique object in its combination of inscriptions on a serpentine block, results of our analyses demonstrate that it conforms to the stylistic conventions, material, and technological methods expected in Middle Formative-period Olmec artifacts. The results of this material research therefore provide a wealth of new contextual information that further supports the authenticity of the object and permit us to better place the CB within the larger context of Olmec cultural traditions, despite its lack of secure provenience. In conjunction with other recent studies (e.g., Mora-Marín 2020), this research strongly supports the identification of the CB as the first known Olmec text, and very likely the first known example of writing in the New World.

In the years since initial doubts were voiced regarding the authenticity, cultural affiliation, and dating of the CB, immediately following publication of its discovery, debate has diminished. Since then, studies of the CB text have conclusively shown that its constituent motifs are consistent with those from contemporaneous iconographic materials and, in some cases, subsequent script traditions (Carrasco and Englehardt 2015; Mora-Marín 2010). Whether or not the CB inscription represents a writing system is one of the few discussions that continues in earnest (see Justeson 2012), but few scholars continue to express doubts about the object's authenticity. Nonetheless, while debate may have receded, the initial doubts concerning the CB have never been conclusively addressed, as the object itself has remained severely understudied.

One of the first to voice skepticism regarding the object was the noted Olmec scholar Cyphers (2007). Although Cyphers (2007:8, translation ours) did not question the capacity of the Olmec culture to have produced either the CB or an independently innovated writing system, she cautions that hasty attributions and conclusions "based on a piece of dubious authenticity [are] not the appropriate way to highlight the achievements of this great culture." She expresses hope, however, that further studies of the artifact will be undertaken to clarify the uncertainties that surround it. Through this research, we have attempted to answer Cyphers' call, providing new data and interpretations that, it is hoped, elucidate some of the doubts, partially fill the lacunae in our understanding, and contribute to increased dialogue and study of the CB. In the end, however, it is clear that further research on the object is necessary to resolve the many issues that continue to surround this singular artifact and its text.

RESUMEN

Este artículo considera el Bloque de Cascajal (CB), un objeto rectangular de piedra verde con incisiones supuestamente proveniente del sur del estado de Veracruz, México. Aunque el CB es un objeto singular que puede contener la escritura más precoz de Mesoamérica, dudas y debates siguen sobre su autenticidad, datación, y filiación cultural. Estas críticas giran, por una parte, en torno a la falta de un contexto arqueológico seguro; por otra, relacionada a las propiedades únicas de su texto, las cuales son distintas a la convención dominante, donde se ordenan los signos en columnas verticales (característica de escrituras mesoamericanas posteriores), así como la singularidad de algunas de las muestras evidentes en el texto inscrito. Aunque su texto ha sido examinado, sorprendentemente no se han realizado investigaciones sobre el soporte en sí, desde la publicación de su hallazgo en 2006.

La investigación de la cual se derive el presente artículo fue diseñada para aportar más datos sobre el CB, un objeto singular cuyo significado es evidente, pero lamentablemente, poco estudiado. Para alcanzar este objetivo, utilizamos varios métodos no-destructivos: (1) Mapeo de Textura Polinomio (PTM), una técnica de fotografía computacional que produce imágenes digitales de alta resolución; (2) análisis espectrométrico por florescencia de rayos X portátil (pFRX); (3) el análisis traceológico vía microscopía electrónica de barrido (MEB) de contramoldes de réplica polímeros que reprodujeron la microestructura superficial del texto inscrito del CB; y (4) el análisis comparativo de trazas de manufactura reveladas a través del análisis MEB con micrografías de muestras de referencia producidas experimentalmente y con otros objetos contemporáneos de procedencia conocida o contexto seguro, previamente analizados con la misma metodología. Este artículo reporta los resultados de estos análisis recientes del CB.

PTM reveló nuevos detalles facilitaron un nuevo dibujo epigráfico del texto inciso del bloque y permitieron una mejor identificación de varios signos constituyentes. El análisis espectrométrico confirmó que la composición mineral de la matriz de CB es consistente con la serpentina e identificó una pátina uniforme en su superficie. Las micrografías MEB de contramoldes de réplica polímeros tomados del texto inciso evidencian trazas de manufactura que corresponden a técnicas lapidarias observadas en otros objetos olmecas de período formativo de procedencia segura.

Así, los resultados de esta investigación demuestran que en términos de material y manufactura, el CB es consistente con otros artefactos olmecas del período Formativo de contexto conocido. Además, los resultados proporcionan evidencia complementaria que clarifican los contextos arqueológicos y la datación del objeto, fortaleciendo los argumentos en apoyo de su autenticidad y afiliación cultural. Estos hallazgos nos permiten colocar al CB firmemente dentro del contexto más amplio de las tradiciones culturales olmecas y reforzar las interpretaciones previas del objeto como el primer ejemplo conocido de la escritura en el Nuevo Mundo.

ACKNOWLEDGMENTS

We thank the community and ejido of Las Lomas de Tacamichapan, Veracruz, as well as the Consejo de Arqueología and Dirección de Registro Público de Monumentos y Zonas Arqueológicos of the Instituto Nacional de Antropología e Historia (INAH), for facilitating access to the Cascajal Block. We also acknowledge the support of INAH's Laboratorio de Microscopía Electrónica, as well as the Museo de Antropología de Xalapa. Finally, we thank Richard Diehl, Lourdes Budar, and Mary Pohl for comments that improved a previous draft of this article. All errors of fact or omission are our own.

Polymer replica molds of the block are archived at INAH Museo del Templo Mayor (MTM) and El Colegio de Michoacán's Laboratorio de

Análisis y Diagnóstico del Patrimonio (LADIPA). Experimentally produced reference materials are housed at INAH MTM, and the raw pXRF data is kept at LADIPA. The CB PTM, as well as the RAW images used to create it and associated metadata, is available by contacting the authors.

This research was supported by funding from El Colegio de Michoacán, A.C., a Florida State University Council for Research and Creativity Planning Grant (2011–2012), INAH, The National Endowment for the Humanities (grant no. HD-51921-14; fellowship no. FA–233454–16), and the Consejo Nacional de Ciencia y Tecnología (grant no. 2015-02-901).

SUPPLEMENTARY MATERIAL

The supplementary material for this article can be found at https://doi.org/10.1017/S0956536119000257.

REFERENCES

Adobe Systems
2019 Adobe DNG Converter 11.1. Electronic program, https://supportdownloads.adobe.com/detail.jsp?ftpID=6529, accessed May 5, 2018.

Alfonso, Juan Andrés, B. Lavelle, Eduardo D. Greaves, and Leonardo Sajó-Bohus
2002 Desarrollo de un método para la determinación de esfuerzos residuales en películas utilizando difracción de rayos-x dispersivo en energía. *Revista latinoamericana de metalurgia y materiales* 22:18–23.

Anderson, Lloyd B.
2012 Understanding Discourse: Beyond Couplets and Calendrics First. In *Parallel Worlds: Genre, Discourse, and Poetics in Contemporary, Colonial, and Classic Period Maya Literature*, edited by Kerry M. Hull and Michael D. Carrasco, pp. 161–179. University Press of Colorado, Boulder.

Andrefsky, William
2006 Experimental and Archaeological Verification of an Index of Retouch for Hafted Bifaces. *American Antiquity* 71:743–757.

Ascher, Robert
1961 Experimental Archaeology. *American Anthropologist* 63:793–816.

Bailey, Scott W.
1969 Polytypism of Trioctahedral 1:1 Layer Silicates. *Clays and Clay Minerals* 17:355–371.

Benavides García, Luis
1983 Domos salinos del sureste de México: Origen, exploración, importancia económica. *Boletín de la Asociación Mexicana de Geólogos Petroleros* 35:9–35.

Bernard, Henri, and Emiliano Melgar
2016 Manufacturing Techniques of Olmec Art Sculptures from Arroyo Pesquero in the MAX (Museo de Antropología de Xalapa). Paper presented at the 81st Annual Meeting of the Society for American Archaeology, Orlando.
2018 Traceology of the Manufacturing Techniques of Olmec Axes. Paper presented at the XVIIIe Congrès Mondial Union Internationale des Sciences Préhistoriques et Protohistoriques, Paris.

Bernard, Henri, Emiliano Melgar, Mayra Manrique, and José Luis Ruvalcaba
2018 El Señor de las Limas: Traceology of the Manufacturing Techniques and Mineralogical Composition. Paper presented at the Association of Archaeological Wear and Residue Analysts, Nice.

Braun, David R., Briana L. Pobiner, and Jessica C. Thompson
2008 An Experimental Investigation of Cut Mark Production and Stone Tool Attrition. *Journal of Archaeological Science* 35:1216–1223.

Bruhns, Karen O., Nancy L. Kelker, Ma. del Carmen Rodríguez Martínez, Ponciano Ortiz Ceballos, Michael D. Coe, Richard A. Diehl, Stephen D. Houston, Karl A. Taube, and Alfredo Delgado Calderón
2007 Did the Olmec Know How to Write? [with response]. *Science* 315: 1365–1366.

Campos Cascaredo, Adolfo
2011 Distribución y caracterización del suelo. In *La biodiversidad en Veracruz: Estudio de estado*, edited by Andrea Cruz Angón, pp. 69–84. Comisión Nacional para el Conocimiento y Uso de la Biodiversidad, Mexico City.

Carrasco, Michael D., and Joshua D. Englehardt
2015 Diphrastic Kennings on the Cascajal Block and the Emergence of Mesoamerican Writing. *Cambridge Archaeological Journal* 25:635–656.

Charlton, Cynthia L. Otis
1993 Obsidian as Jewelry: Lapidary Production in Aztec Otumba, Mexico. *Ancient Mesoamerica* 4:231–243.

Cultural Heritage Imaging (CHI)
2011 RTI Guide to Highlight Image Capture. Electronic document, http://culturalheritageimaging.org/What_We_Offer/Downloads/RTI_Hlt_Capture_Guide_v2_0.pdf, accessed May 5, 2018.
2013 RTI Guide to Highlight Image Processing. Electronic document, http://culturalheritageimaging.org/What_We_Offer/Downloads/rtibuilder/RTI_hlt_Processing_Guide_v14_beta.pdf, accessed May 5, 2018.
2017 RTI Builder software. Electronic document, http://culturalheritageimaging.org/What_We_Offer/Downloads/Process/index.html, accessed May 18, 2017.
2018 Reflectance Transformation Imaging (RTI). Electronic document, http://culturalheritageimaging.org/Technologies/RTI, accessed May 5, 2018.

Cyphers, Ann
2007 Sobre el bloque labrado de El Cascajal, Jáltipan, Veracruz. *Arqueología mexicana* 14:6–8.

Diaz-Guardamino, Marta, and David Wheatley
2013 Rock Art and Digital Technologies: The Application of Reflectance Transformation Imaging (RTI) and 3D Laser Scanning to the Study of Late Bronze Age Iberian Stele. *Menga: Revista de prehistoria de Andalucía* 4:187–203.

Dong, Mei, Zhibao Li, Jianguo Mi, and George P. Demopoulos
2009 Solubility and Stability of Nesquehonite ($MgCO_3 \bullet 3H_2O$) in Mixed $NaCl + MgCl_2$, $NH_4Cl + MgCl_2$, LiCl, and $LiCl + MgCl_2$ Solutions. *Journal of Chemical and Engineering Data* 54:3002–3007.

Drucker, Philip
1952 *La Venta Tabasco: A Study of Olmec Ceramics and Art*. Smithsonian Institution Bureau of American Ethnology Bulletin 153. Smithsonian Institution, Washington, DC.

Drucker, P. Philip, Robert F. Heizer, and Robert J. Squier
1959 *Excavations at La Venta, Tabasco, 1955*. Smithsonian Institution Bureau of American Ethnology Bulletin 170. United States Government Printing Office, Washington, DC.

Durán, Fray Diego
1967 *Historia de las indias de Nueva España e islas de Tierra Firme*. Editorial Porrúa, Mexico City.

Earl, Graeme, Kirk Martinez, and Tom Malzbender
2010 Archaeological Applications of Polynomial Texture Mapping: Analysis, Conservation and Representation. *Journal of Archaeological Science* 37:2040–2050.

Englehardt, Joshua D., Michael D. Carrasco, and Mary E.D. Pohl
2017 Nuevos trazos de la cultura visual olmeca: La aplicación de técnicas digitales de visualización. In *Arqueología de la Costa del Golfo. Dinámicas de la interacción política, económica e ideológica*, edited by Lourdes Budar Jiménez, Marcie Venter, and Sara Ladrón de Guevara, pp. 349–366. Universidad Veracruzana, Xalapa.

Eren, Metin I., Stephen J. Lycett, Robert J. Patten, Briggs Buchanan, Justin Pargeter, and Michael J. O'Brien
2016 Test, Model, and Method Validation: The Role of Experimental Stone Artifact Replication in Hypothesis-Driven Archaeology. *Ethnoarchaeology* 8:103–136.

Esteves Teixeira, Carlos
2016 *Estrutura e estabilidade dos politipos dos filossilicatos 1:1 por primeiros principios*. Unpublished Ph.D. dissertation, Universidad Federal de Minas Gerais, Brazil.

Fandeur, Dik, Farid Juillot, Guillaume Morin, Luca Olivi, Andrea Cognigni, Samuel M. Webb, Jean-Pauñ Ambrosi, Emmanuel Fritsch, François Guyot, and Gordon E. Brown, Jr.
2009 XANES Evidence for Oxidation of Cr(III) to Cr(VI) by Mn-oxides in a Lateritic Regolith Developed on Serpentinized Ultramafic Rocks of New Caledonia. *Environmental Science and Technology* 43:7384–7390.

Feinman, Gary M., and Linda M. Nicholas
1995 Household Craft Specialization and Shell Ornament Manufacture in Ejutla, México. *Expedition* 37:14–25.

Freidel, David A., and F. Kent Reilly III
2010 The Flesh of God: Cosmology, Food, and the Origins of Political

Power in Ancient Southeastern Mesoamerica. In *Pre-Columbian Foodways: Interdisciplinary Approaches to Food, Culture, and Markets in Ancient Mesoamerica*, edited by John Staller and Michael D. Carrasco, pp. 635–680. Springer, New York.

Fryer, Patricia, and Michael J. Mottl
1992 Lithology, Mineralogy and Origin of Serpentine Muds Recovered from Conical and Torishima Forearc Seamounts: Results of Leg 125 Drilling. In *Proceedings of the Ocean Drilling Program, Scientific Results, Vol. 125*, edited by Patricia Fryer, Patrick Coleman, Julian A. Pearce, and Laura B. Stokking, pp. 343–362. Ocean Drilling Program, Texas A&M University, College Station.

Hewlett-Packard Laboratories (HP Labs)
2019a Highlight-based PTMs. Electronic document, https://www.hpl.hp.com/research/ptm/HighlightBasedPtms/index.html, accessed November 7, 2019.
2019b Making PTMs. Electronic document, https://www.hpl.hp.com/research/ptm/MakingPtmNew.htm, accessed November 7, 2019.

Houston, Stephen D.
2004 Writing in Early Mesoamerica. In *The First Writing: Script Invention as History and Process*, edited by Stephen D. Houston, pp. 274–309. Cambridge University Press, Cambridge.

Instituto Nacional de Estadística y Geografía (INEGI)
2019 Edafología. Electronic document, https://www.inegi.org.mx/temas/edafologia, accessed January 8, 2019.

Justeson, John S.
2012 Early Mesoamerican Writing Systems. In *The Oxford Handbook of Mesoamerican Archaeology*, edited by Deborah L. Nichols, pp. 830–844. Oxford University Press, Oxford.

Konrad-Schmolke, Matthias, Ralf Halama, Richard Wirth, Aurélien Thomen, Nico Klitscher, Luiz Morales, Anja Schreiber, and Franziska D. H. Wilke
2018 Mineral Dissolution and Reprecipitation Mediated by an Amorphous Phase. *Nature Communications* 9:1637.

Krevor, Samuel C.M., and Klaus S. Lackner
2011 Enhancing Serpentine Dissolution Kinetics for Mineral Carbon Dioxide Sequestration. *International Journal of Greenhouse Gas Control* 5:1073–1080.

Laughlin, John P., and Robert L. Kelly
2010 Experimental Analysis of the Practical Limits of Lithic Refitting. *Journal of Archaeological Science* 37:427–433.

Lerner, Harry J.
2013 Experiments and Their Application to Lithic Archaeology: An Experimental Essay. In *Human Expeditions: Inspired by Bruce Trigger*, edited by Stephen Chrisomalis and Andre Costopoulos, pp. 73–89. University of Toronto Press, Toronto.

Li, Xiuzhen Janice, Marcos Martinón-Torres, Nigel D. Meeks, Yin Xia, and Kun Zhao
2011 Inscriptions, Filing, Grinding and Polishing Marks on the Bronze Weapons from the Qin Terracotta Army in China. *Journal of Archaeological Science* 38:492–501.

López Portillo, Jorge, Maria Luisa Martínez, Patrick A. Hesp, José Ramón Hernández, Ana Patricia Méndez, Victor M. Vásquez-Reyes, León Rodrigo Gómez Aguilar, Oscar A. Jiménez-Orocio, and Sheila L. Gachuz Delgado
2011 *Atlas de las costas de Veracruz: Manglares y dunas costeras*. Secretaría de Educación del Estado de Veracruz, Veracruz.

Macri, Martha J.
2006 The Cascajal Block: Sign Ordering. *Glyph Dwellers* 22:1–4.

Magni, Caterina
2008 Olmec Writing. The Cascajal Block: New Perspectives. *Arts and Cultures* 9:64–81.
2014 *Les Olmèques. La genèse de l'ecriture en meso-amerique*. Errance, Paris.

Malzbender, Tom, Dan Gelb, and Hans Wolters
2001 Polynomial Texture Maps. In *SIGGRAPH '01: Proceedings of the 28th Annual Conference on Computer Graphics and Interactive Techniques*, pp. 519–528. ACM Press, New York.

Marsh, Erik J., and Jeffrey R. Ferguson
2010 Introduction. In *Designing Experimental Research in Archaeology: Examining Technology through Production and Use*, edited by Jeffrey R. Ferguson, pp. 1–13. University Press of Colorado, Boulder.

McPherron, Shannon P., David. R. Braun, Tamara Dogandžića, Will Archer, Dawit Desta, and Sam C. Lin
2014 An Experimental Assessment of the Influences on Edge Damage to Lithic Artifacts: A Consideration of Edge Angle, Substrate Grain Size, Raw Material Properties, and Exposed Face. *Journal of Archaeological Science* 49:70–82.

Melgar Tísoc, Emiliano R.
2017 Manufacturing Techniques of Greenstone Mosaics from Teotihuacan and Palenque. In *Playing with the Past. Experimental Archaeology and the Study of the Past*, edited by Rodrigo Alonso, David Canales, and Javier Baena, pp. 119–124. Universidad Autónoma de Madrid, Madrid.

Melgar Tísoc, Emiliano R., and Reyna Beatríz Solís Ciriaco
2005 Arqueología experimental en lapidaria en el Templo Mayor de Tenochtitlán. *Actualidades arqueológicas* 6, https://revistas.uam.es/index.php/arqexp/article/view/5776/6225.

Melgar Tísoc, Emiliano R., and Reyna Beatríz Solís Ciriaco
2009 Caracterización de huellas de manufactura en objetos lapidarios de obsidiana del Templo Mayor de Tenochtitlan. *Arqueología* 42: 118–134.
2015 The Technological Analysis of Lapidary Objects from Tenochtitlan. In *Breaking Barriers: Proceedings of the 47th Annual Chacmool Archaeological Conference*, edited by Robyn Crook, Kim Edwards, and Colleen Hughes, pp. 118–128. University of Calgary, Calgary.
2017 Los objetos lapidarios de "estilo mixteco" en el Templo Mayor de Tenochtitlan. Sus características tecnológicas. In *Estilo y región en el arte mesoamericano*, edited by María Isabel Álvarez Icaza and Pablo Escalante Gonzalbo, pp. 263–282. Universidad Nacional Autónoma de México, Mexico City.
2018 Caracterización mineralógica y tecnológica de la lapidaria de Teopancazco. In *Teopancazco como centro de barrio multiétnico de Teotihuacan. Los sectores funcionales y el intercambio a larga distancia*, edited by Linda Manzanilla, pp. 621–672. Universidad Nacional Autónoma de México, Mexico City.

Melgar Tísoc, Emiliano R., Reyna Beatríz Solís Ciriaco, and Ernesto González Licón
2010 Producción y prestigio en concha y lapidaria de Monte Albán. In *Producción de bienes de prestigio ornamentales y votivos de la América antigua*, edited by Emiliano R. Melgar Tísoc, Reyna Beatríz Solís Ciriaco, and Ernesto González Licón, pp. 7–22. Syllaba Press, Miami.

Melgar Tísoc, Emiliano R., Reyna Beatríz Solís Ciriaco, and Hervé V. Monterrosa Desruelles
2018 *Piedras de fuego y agua. Turquesas y jades entre los Nahua*. Universidad Nacional Autónoma de México Museo de Geología, Mexico City.

Melgar Tísoc, Emiliano R., Reyna Beatríz Solís Ciriaco, and José Luis Ruvalcaba
2012 Technological and Material Characterization of Lapidary Artifacts from Tamtoc Archaeological Site, Mexico. *Materials Research Society Symposium Proceedings* 1374:103–114.

Mendoza Cuevas, Adriana, and Homero Pérez Gravie
2011 Portable Energy Dispersive X-Ray Fluorescence and X-Ray Diffraction and Radiography System for Archaeometry. *Nuclear Instruments and Methods in Physics Research Section A: Accelerators, Spectrometers, Detectors and Associated Equipment* 633:72–78.

Mercy, Edward, and Michael J. O'Hara
1967 Distribution of Mn, Cr, Ti and Ni in Co-existing Minerals of Ultramafic Rocks. *Geochimica et Cosmochimica Acta* 31:2331–2341.

Mirambell, Lorena
1968 *Técnicas Lapidarias Prehispánicas*. Instituto Nacional de Antropología e Historia, Mexico City.

Moholy-Nagy, Hattula
1997 Middens, Construction Fill, and Offerings: Evidence for the Organization of Classic Period Craft Production at Tikal, Guatemala. *Journal of Field Archaeology* 24:293–313.

Monterrosa Desruelles, Hervé V., and Emiliano R. Melgar Tísoc
2017 Reliquias mayas y olmecas de jadeíta en el Templo Mayor de Tenochtitlan. In *XXX Simposio de investigaciones arqueológicas en Guatemala, 2016, Tomo II*, edited by Bárbara Arroyo, Luis Méndez, and Gloria Ajú, pp. 905–916. Instituto Nacional de Antropología e Historia, Museo Nacional de Arqueología y Etnología, Guatemala City.

Mora-Marín, David
2009 Early Olmec Writing: Reading Format and Reading Order. *Latin American Antiquity* 20:395–412.

2010 *Further Analysis of Olmec Writing on the Cascajal Block: Sign Inventory, Paleography, Script Affiliations*. Unpublished manuscript in possession of the authors.
2020 The Cascajal Block: New Line Drawing, Distributional Analysis, Orthographic Patterns. *Ancient Mesoamerica*. Forthcoming, doi: 10.1017/S0956536119000270.

Nami, Hugo G.
2010 Theoretical Reflections on Experimental Archaeology and Lithic Technology: Issues on Actualistic Stone Tools Analysis and Interpretation. In *Experiments and Interpretation of Traditional Technologies: Essays in Honor of Errett Callahan*, edited by Hugo G. Nami, pp. 91–168. Ediciones de Arqueología Contemporánea, Buenos Aires.

Ortiz Ceballos, Ponciano, Ma. del Carmen Rodríguez Martínez, Ricardo Sánchez Hernández, and Jasinto Robles Camacho
2007 El bloque labrado con inscripciones olmecas. *Arqueología Mexicana* 83:15–18.

Ortiz Hernández, Luis Enrique, José Cruz Escamilla Casas, Kinardo Flores Castro, Marius Ramírez Cardona, and Otilio Acevedo Sandoval
2006 Características geológicas y potencial metalogenético de los principales complejos ultramáficos-máficos de México. *Boletín de la Sociedad Geológica Mexicana* 58:161–181.

Oze, Christopher, Scott Fendorf, Dennis K. Bird, and Robert G. Coleman
2004 Chromium Geochemistry in Serpentinized Ultramafic Rocks and Serpentine Soils from the Franciscan Complex of California. *American Journal of Science* 304:67–101.

Pérez Jiménez, José Luis
2010 *Sedimentología, silicificaciones y otros procesos diagenéticos en las unidades intermedia y superior del Mioceno de la Cuenca de Madrid (zonas NE, NW y W)*. Unpublished Ph.D. dissertation, Universidad Complutense de Madrid, Madrid.

Purdy, Barbara A., Kevin S. Jones, John J. Mecholsky, Gerald Bourne, Richard C. Hulbert, Bruce J. MacFadden, Krista L. Church, Michael W. Warren, Thomas F. Jorstad, Dennis J. Stanford, Melvin J. Wachowiak, and Robert J. Speakman
2011 Earliest Art in the Americas: Incised Image of a Proboscidean on a Mineralized Extinct Animal Bone from Vero Beach, Florida. *Journal of Archaeological Science* 38:2908–2913.

Putt, Shelby S.
2015 The Origins of Stone Tool Reduction and the Transition to Knapping: An Experimental Approach. *Journal of Archaeological Science Reports* 2:51–60.

Puy y Alquiza, María Jesús
2017 *Reporte petrográfico. Jade*. Manuscript on file, Archivo del Laboratorio de Petrología, Facultad de Minas, Metalurgia y Geología, Universidad de Guanajuato, Guanajuato.

Ritger, Scott, Bobb Carson, and Erwin Suess
1987 Methane-Derived Authigenic Carbonates Formed by Subduction-Induced Pore-Water Expulsion along the Oregon/Washington Margin. *Geological Society of America Bulletin* 98:147–156.

Robles Camacho, Jacinto, Hermann Köhler, Peter Schaaf, and Ricardo Sánchez Hernández
2008 *Serpentinas olmecas: Petrología aplicada a la arqueometría*. Monografías del Instituto de Geofísica No. 13. Universidad Nacional Autónoma de México, Mexico City.

Rodríguez Martínez, Ma. del Carmen, and Ponciano Ortiz Ceballos
1999 Informe de inspección en la zona de El Cascajal, municipio de Jáltipan, Veracruz. Manuscript on file, Archivo Técnico del Centro INAH Veracruz, Veracruz.
2007 El bloque labrado con símbolos olmecas encontrado en El Cascajal, municipio de Jáltipan, Veracruz. *Arqueología* 36:24–51.

Rodríguez Martínez, Ma. del Carmen, Ponciano Ortiz Ceballos, Michael D. Coe, Richard A. Diehl, Stephen D. Houston, Karl A. Taube, and Alfredo Delgado Calderón
2006 Oldest Writing in the New World. *Science* 313:1610–1614.

Ruttenberg, Kathleen C., and Robert A. Berner
1993 Authigenic Apatite Formation and Burial in Sediments from Non-Upwelling, Continental Margin Environments. *Geochimica et Cosmochimica Acta* 57:991–1007.

Sahagún, Fray Bernardino de
1956 *Historia general de las cosas de Nueva España*. Editorial Porrúa, Mexico City.

Sanna, Aimaro, Luc Steel, and M. Mercedes Maroto-Valer
2017 Carbon Dioxide Sequestration Using $NaHSO_4$ and NaOH: A Dissolution and Carbonation Optimization Study. *Journal of Environmental Management* 189:84–97.

Sax, Margaret, Nigel D. Meeks, Carol Michaelson, and Andrew P. Middleton
2004 The Identification of Carving Techniques on Chinese Jade. *Journal of Archaeological Science* 31:1414–1428.

Skidmore, Joel
2006 *The Cascajal Block: The Earliest Precolumbian Writing*. Electronic document, www.mesoweb.com/reports/Cascajal.pdf, accessed November 30, 2018.

Solís Ciriaco, Reyna Beatriz, Emiliano Ricardo Melgar Tísoc, and Lynneth Lowe
2016 Análisis Tecnológico de las Hachas de Piedra Verde de Chiapa de Corzo. In *XXIX simposio de investigaciones arqueológicas de Guatemala*, pp. 1087–1097. Museo Nacional de Arqueología y Etnología, Guatemala City.

Solís Ciriaco, Reyna Beatríz, and Emiliano R. Melgar Tísoc
2017 Technological Analysis of Greenstone Objects from the structures surrounding the great temple of Tenochtitlán. In *Playing with the Past. Experimental Archaeology and the Study of the Past*, edited by Rodrigo Alonso, David Canales, and Javier Baena, pp. 125–130. Universidad Autónoma de Madrid, Madrid.

Steyn, Ruan
2014 *Portable X-Ray Fluorescence and Nuclear Microscopy Techniques Applied to the Characterization of Southern African Rock Art Paintings*. Master's thesis, Faculty of Science, Stellenbosch University, Stellenbosch.

Thermo Fisher Scientific
2011 *User's Guide: Thermo Fisher Scientific NITON Analyzers: XL3 Version 8.0.0*. Thermo Fisher Scientific, Waltham.

Valdivia García, Giselle, Milady Arostegui, José A. Alonso Pérez, Ileana Cabrera, Nayda A. Hernández, Victoria Herrera, Carlos Cruz, Abdel Casanova, Asor Martínez, Nery Díaz, and Antonio Aguila
2014 Actualización del conocimiento mineralógico de menas lateríticas y residuos sólidos de las industrias niquelíferas Cubanas. *INFOMIN* 6: 70–100.

Velázquez Castro, Adrian
2007 *La producción especializada de los objetos de concha del Templo Mayor de Tenochtitlan*. Instituto Nacional de Antropología e Historia, Mexico City.

Velázquez Maldonado, Luis Ramón
2017 *Obsidiana y productores especializados en la subregión del Lerma Medio: Estudio de procedencia y patrones de distribución*. Master's thesis, Centro de Estudios Arqueológicos, El Colegio de Michoacán, La Piedad.

Walsh, Jane M.
2008 The Dumbarton Oaks Tlazolteotl: Looking Beneath the Surface. *Journal de la Société des Américanistes* 94:7–43.

Wendt, Carl J., Henri N. Bernard, and Jeffery Delsescaux
2014 A Middle Formative Artifact Excavated at Arroyo Pesquero, Veracruz. *Ancient Mesoamerica* 25:309–316.

Winfield Capitaine, Fernando
1988 *La Estela 1 de La Mojarra, Veracruz*. Research Reports on Ancient Maya Writing, Publication 16. Center for Maya Research, Washington, DC.